The fast matched filter for gravitational-wave data analysis: Characteristics and applications

P. ASTONE ([1]), C. BUTTIGLIONE ([2]), S. FRASCA ([3])
G. V. PALLOTTINO ([3]) and G. PIZZELLA ([4])
([1]) *INFN, Sezione di Roma 1 - Roma, Italy*
([2]) *CIRG - Roma, Italy*
([3]) *Dipartimento di Fisica "La Sapienza", INFN, Sezione di Roma 1 - Roma, Italy*
([4]) *Dipartimento di Fisica "Tor Vergata", INFN, LNF - Roma, Italy*

(ricevuto il 19 Luglio 1996; approvato l'11 Ottobre 1996)

Summary. — We report on the application of a matched filter to the data of two-mode resonant gravitational-wave antennas for the detection of burst signals, with reference to data obtained by direct acquisition, *i.e.* without going through lock-in amplifiers, sampled at relatively high speed. After a review of the basic model of resonant detectors, that includes a discussion of the signal and of the noise, we present a detailed mathematical derivation of the optimum filter matched to an input burst. We then analyze and discuss the performance of the matched filter as regards both the improvement of the signal-to-noise ratio and the observation bandwidth, also considering the adaptive realization of the filter, based on the actual spectrum of the noise as estimated from the data. The discussion that follows is centered on various aspects concerning the practical application of the matched filter as well as the loss of performance due both to uncertainties on the parameters used for building the filter and to various discretization effects, both in the time and frequency domains. Finally, we consider some experimental results obtained by applying the matched filter to the data of the Explorer detector, also providing a comparison with what we obtained by applying an optimum filter to data processed by lock-in amplifiers, sampled at lower speed.

PACS 04.80 – Experimental studies of gravity.

1. – The experimental apparatus

1˙1. *Model of the bar-transducer system.* – We consider a cylindrical gravitational-wave antenna of mass M and length L, whose vibrations are observed at the frequency of its first longitudinal mode ν_x, which is coupled to the gravitational radiation field. The vibrations of the bar are converted into an electrical signal by an electromechanical transducer of mass M_t, resonating at the antenna frequency in order to improve the energy transfer from the bar to the electronics. The capacitive transducer

is bolted to one end of the antenna, and consists of a fixed plate and of a vibrating disk. The transduction constant α between the disk vibrations and the output voltage is

$$\alpha = \gamma_t \frac{V_b}{d} \quad (\mathrm{V/m}), \tag{1.1}$$

where d is the transducer gap, V_b the bias voltage and γ_t is a geometrical factor, typically $\simeq 0.85$. The transducer output signal is connected to a d.c. SQUID amplifier through a decoupling capacitance and a superconducting transformer used to obtain the proper matching between the high impedance of the transducer and the low impedance of the input coil of the SQUID.

The bar, the resonant trasducer and the LC electrical circuit at the transducer output form a system of three coupled oscillators: Two mechanical oscillators, the bar at frequency ν_x and the transducer at frequency ν_y; one electrical oscillator, the LC circuit with resonance frequency ν_{el}. Since this work aims at clarifying the operation of the filters used to analyse the data, we shall consider a specific particular case, for which the mathematical treatment is greatly simplified. We assume in the following:

a) that the frequency of the electrical oscillator is sufficiently larger than those of the mechanical oscillators ($\nu_{el} \gg \nu_x, \nu_y$) so that we can neglect its effect on the dynamical behaviour of the system;

b) that the frequencies of the two mechanical oscillators are very close, *i.e.* $\nu_y \simeq \nu_x$ (within few Hz), as required for optimum energy coupling.

We consider, therefore, a two-mode approximation for the three-mode detection system, which turns out to be very accurate for representing the experimental behavior of the antenna EXPLORER [1].

The block diagram of the experimental apparatus of this detector is shown in fig. 1. The signal at the SQUID output is processed by means of two different procedures: 1) it is first filtered with a bandpass filter with flat response in the frequency range (902–926) Hz, that includes the resonances of the two modes, and strong attenuation outside, and then it is directly sampled at the rate of 220 Hz ($\Delta t = 4.5$ ms). As a result, the signals in the region of our interest between 900 and 927.5 Hz are transposed in the range 20–47.5 Hz. 2) It is sent to four lock-in amplifiers ([1]), whose outputs are sampled at a much slower rate, 0.34 Hz ($\Delta t = 0.290$ s).

The lock-in amplifiers demodulate the signal at the frequencies of the two resonance modes, ν_- and ν_+, at the frequency of the calibration signal ([2]) used to monitor the gain of the SQUID, and at a frequency in the region between the two modes that provides information on the wide-band noise.

Figure 2 shows the model of the bar-transducer system. The mechanical parameters of the bar and of the transducer oscillators are the reduced masses $m_x = M/2$, $m_y = \gamma_t M_t$, the stiffnesses $k_x = m_x \omega_x^2$, $k_y = m_y \omega_y^2$ and the dissipation coefficients β_x, β_y.

([1]) A lock-in amplifier extracts the Fourier component of the input signal at a chosen frequency: the two output signals of a lock-in are proportional to the real and imaginary part of the complex oscillation of the observed antenna mode.

([2]) Since the gain of the SQUID amplifier, that is the slope of its V/ϕ characteristics, may be not constant in time, it is continuously monitored by applying a reference magnetic field at a frequency ν_{cal}. The corresponding output signal is used to normalize the data.

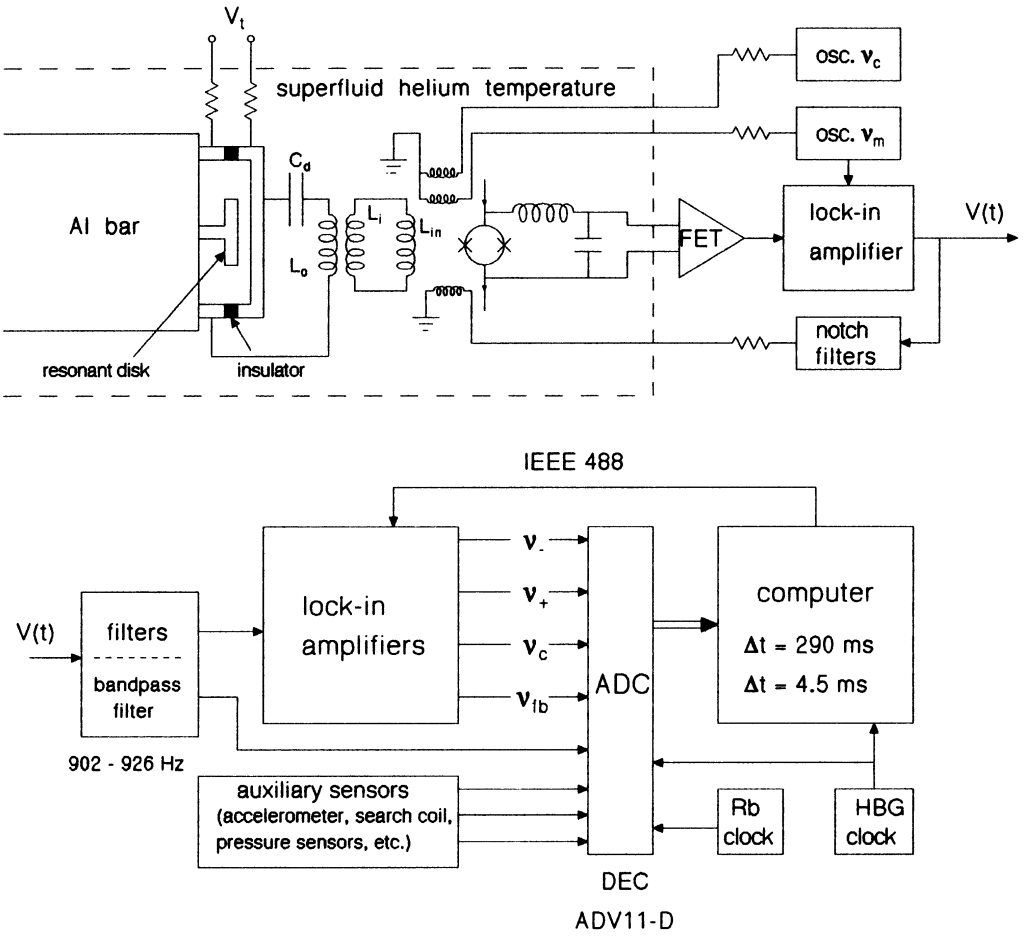

Fig. 1. – Block diagram of the experimental apparatus.

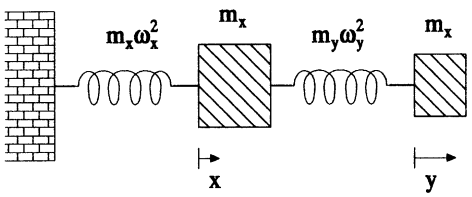

Fig. 2. – Model of the bar-transducer system.

The bar and the transducer are considered as point-like masses, with displacements $x(t)$ and $y(t)$ from their equilibrium positions. The electrical output of the transducer is proportional to the difference between the displacements of the bar and of the transducer, $u(t) = y(t) - x(t)$.

If $f_x(t)$ and $f_y(t)$ are external forces, acting, respectively, on the masses m_x and m_y, then the equations representing the system are [2-4]

$$m_x\ddot{x} + m_x\omega_x^2 x + 2m_x\beta_x\dot{x} + m_y\omega_y^2(x-y) + 2m_y\beta_y(\dot{x}-\dot{y}) = f_x, \tag{1.2}$$

$$m_y\ddot{y} + m_y\omega_y^2(y-x) + 2m_y\beta_y(\dot{y}-\dot{x}) = f_y. \tag{1.3}$$

Using the Fourier transforms, we derive

$$X(j\omega) = F_x(j\omega)W_{xx}(j\omega) + F_y(j\omega)W_{xy}(j\omega),$$

$$Y(j\omega) = F_x(j\omega)\,W_{yx}(j\omega) + F_y(j\omega)\,W_{yy}(j\omega),$$

where the transfer functions from the forces to the displacements are

$$W_{xx}(j\omega) = \frac{-\omega^2 + \omega_y^2 + 2j\omega\beta_y}{m_x D(j\omega)}, \tag{1.4}$$

$$W_{yy}(j\omega) = \frac{-\omega^2 + \omega_x^2 + \mu\omega_y^2 + 2j\omega(\beta_x + \mu\beta_y)}{m_y D(j\omega)}, \tag{1.5}$$

$$W_{xy}(j\omega) = W_{yx}(j\omega) = \frac{\omega_y^2 + 2j\omega\beta_y}{m_x D(j\omega)}, \tag{1.6}$$

with

$$\mu = \frac{m_y}{m_x}, \tag{1.7}$$

$$D(j\omega) = \omega^4 - j\omega^3 A + \omega^2 B + j\omega C + \omega_x^2\omega_y^2, \tag{1.8}$$

$$\begin{cases} A = 2[(\beta_x + \mu\beta_y) + \beta_y], \\ B = -\omega_x^2 - \omega_y^2(\mu+1) - 4\mu\beta_y^2 - 4\beta_y\beta_x(\mu+1), \\ C = 2\omega_y^2(\beta_x + \mu\beta_y - \mu\beta_x) + 2\beta_y\omega_x^2. \end{cases} \tag{1.9}$$

For the signal $u(t) = y(t) - x(t)$ the transfer functions are

$$W_{ux}(j\omega) = \frac{U(j\omega)}{F_x(j\omega)} = \frac{\omega^2}{m_x D(j\omega)}, \tag{1.10}$$

$$W_{uy}(j\omega) = \frac{U(j\omega)}{F_y(j\omega)} = \frac{-\omega^2 + \omega_x^2 + 2j\omega\beta_x}{m_y D(j\omega)}. \tag{1.11}$$

For a system without dissipations ($\beta_x = \beta_y = 0$) it is possible to derive a simple solution of the equation $D(j\omega) = 0$, obtaining the following expression for the

resonance frequencies of the two modes

$$\omega_{\pm}^2 = \frac{\omega_x^2 + \omega_y^2(1+\mu) \pm \sqrt{[\omega_x^2 + \omega_y^2(1+\mu)]^2 - 4\omega_x^2\omega_y^2}}{2} . \tag{1.12}$$

In the case of perfect tuning of the bar and the tranducer ($\omega_x = \omega_y = \omega_0$) we obtain

$$\omega_{\pm} = \omega_0 \sqrt{1 + \frac{\mu}{2} \pm \sqrt{\mu + \frac{\mu^2}{4}}}$$

and, being $\mu \ll 1$,

$$\omega_{\pm} \simeq \omega_0 \left(1 \pm \frac{\sqrt{\mu}}{2}\right). \tag{1.13}$$

In this case the quantity $\omega_+^2 - \omega_-^2$ is minimum:

$$\omega_+^2 - \omega_-^2 = 2\sqrt{\mu}\,\omega_0^2 \sqrt{(1+\mu/2)} \simeq 2\omega_0^2\sqrt{\mu} \tag{1.14}$$

and the energy transfer between the two coupled oscillators is total. The energy transfer is, however, still close to the maximum, and the above approximation holds, when

$$|\omega_x - \omega_y| \ll (\omega_x + \omega_y)\sqrt{\mu}/4 , \tag{1.15}$$

which we assume as the practical tuning condition for all the considerations that follow.

If we consider the dissipations, eq. (1.13) is still valid with very good accuracy because in the cases of our interest $\beta_x, \beta_y \ll \omega_x, \omega_y$, being $Q_x, Q_y \gg 1$. The merit factors Q_x and Q_y of the two uncoupled oscillators are

$$Q_{x,y} = \frac{\omega_{x,y}}{2\beta_{x,y}} , \tag{1.16}$$

those of the modes of the coupled system

$$Q_{\pm} = \frac{\omega_{\pm}}{2\beta_{\pm}} . \tag{1.17}$$

For a very tight coupling of the oscillators, $\beta_- = \beta_+ = \beta_0$.

1˙2. *The signal.* – We consider here the detector response to a short gravitational-wave (g.w.) pulse. We assume the detector at rest and we model the excitation as an impulse force

$$f_x(t) = f_0 \tau \delta(t) \tag{1.18}$$

applied to the bar (m_x) oscillator, whose coefficient can be expressed as a product of an

intensity f_0 ([3]) and of a duration τ. We remark that the input delta-function assumption is only valid if the time duration of the applied force is small compared with all the time constants of the apparatus and of the filters used in the data analysis procedures, as well as with the reciprocal of the observation bandwidth of interest.

According to the above assumptions, at the time of application of the input force the energy E_s of the g.w. burst absorbed by the detector is totally converted into kinetic energy of the bar oscillator, that is

$$E_s = E_x = \frac{1}{2}\,\frac{(f_0\tau)^2}{m_x}\,, \tag{1.19}$$

from which we derive

$$f_0\tau = \sqrt{2E_s m_x}. \tag{1.20}$$

The transducer displacement is obtained by antitransforming the equation $U(j\omega) = W_{ux}(j\omega)\,F_x(j\omega)$ (see eq. (1.10))

$$u_{\mathrm{sig}}(t) = \frac{f_0\tau}{m_x(\omega_+^2 - \omega_-^2)}\,[\omega_+ \exp[-\beta_+ t]\sin\omega_+ t - \omega_- \exp[-\beta_- t]\sin\omega_- t] \tag{1.21}$$

and the corresponding signal at the transducer output is

$$V_{t_{\mathrm{sig}}}(t) = \frac{\alpha f_0\tau}{m_x(\omega_+^2 - \omega_-^2)}\,[\omega_+ \exp[-\beta_+ t]\sin\omega_+ t - \omega_- \exp[-\beta_- t]\sin\omega_- t]\,. \tag{1.22}$$

1·3. *The noise.* – The Brownian noise, that is the thermal noise of the two mechanical oscillators, is evaluated by using the generalized Nyquist theorem which associates to each dissipative element a noise generator of suitable power spectral density. The mechanical dissipations $2\beta_x/m_x$, $2\beta_y/m_y$ correspond to noise force generators with two-sided spectral density

$$S'_{fx} = 4kT\beta_x m_x, \qquad S'_{fy} = 4kT\beta_y m_y, \tag{1.23}$$

where $k = 1.38\cdot 10^{-23}$ is the Boltzmann constant and T is the thermodynamical temperature. The corresponding spectral densities of the displacement $u(t)$ are, therefore, given by

$$S_{ux} = S'_{fx}\,|W_{ux}(j\omega)|^2, \qquad S_{uy} = S'_{fy}\,|W_{uy}(j\omega)|^2. \tag{1.24}$$

The back-action effect of the amplifier noise through the transducer on the mechanical oscillators may be expressed by a random force $f_n(t)$ with spectrum $S_f(\omega)$. If this spectrum is flat, under reasonable assumptions discussed in [5], we can write the total noise force spectra, due to both the Nyquist and the back-action force, as

$$S_{fx} = 4kT_e\beta_x m_x, \qquad S_{fy} = 4kT_e\beta_y m_y, \tag{1.25}$$

([3]) For a short burst of g.w. of amplitude h_0 at ω_0 we have $f_0 = 2m_x L\omega_0^2 h_0/\pi^2$, where L is the length of the bar.

where we have introduced the *equivalent temperature* T_e, defined as the temperature which would provide the same output noise as given by both the Nyquist force and the back-action. The total narrow-band noise spectrum, at the transducer output, is

$$S_{nb}(\omega) = \alpha^2 S_{fx} |W_{ux}(j\omega)|^2 + \alpha^2 S_{fy} |W_{uy}(j\omega)|^2 \tag{1.26}$$

and the corresponding mean-square voltages for the two modes are

$$V^2_{br_\pm} = 4kT_e\alpha^2(|W_{ux}(j\omega_\pm)|^2 m_x\beta_x + |W_{uy}(j\omega_\pm)|^2 m_y\beta_y)\beta_\pm . \tag{1.27}$$

It can be demonstrated that (1.27) can be simplified as follows when the tuning condition between the bar and the transducer is fulfilled:

$$V^2_{br_\pm} = \alpha^2 \frac{kT_e}{2m_y\omega^2_\pm} . \tag{1.28}$$

The signal-to-noise ratio is usually defined in terms of mean-square values. Here we consider it more convenient to express this quantity in terms of the ratio between the square of the maximum of the signal and the mean-square value of the noise.

When the tuning condition is fulfilled, for a signal of energy $E_s = kT_s$, we have from eqs. (1.20) and (1.22)

$$V^2_{t_{max}} \simeq \frac{2\alpha^2 kT_s}{m_y\omega^2_0} . \tag{1.29}$$

The total narrow-band noise variance is

$$\sigma^2_{nb} = V^2_{br_-} + V^2_{br_+} \simeq \frac{\alpha^2 kT_e}{m_y\omega^2_0} ; \tag{1.30}$$

the signal-to-noise ratio is therefore

$$(SNR)_0 = V^2_{t_{max}}/\sigma^2_{nb} = 2T_s/T_e , \tag{1.31}$$

which means that the square of the peak value of the signal is twice the mean square value of the noise for a signal having the same energy as the noise.

1·4. *Model of the electrical circuit and of the* SQUID. – Figure 3 represents the electrical circuit from the transducer to the SQUID amplifier. C_t and C_p are the transducer active and parasitic capacitances; C_d is the decoupling capacitance. The transformer has primary inductance L_0, secondary inductance L_s, with turn ratio $N = \sqrt{L_0/L_s}$. L_{in} is the inductance of the input coil of the SQUID, coupled through the mutual inductance M.

We analyze the circuit obtaining the following expression for the current I flowing through the input coil of the SQUID:

$$I(j\omega) = V_t(j\omega) \frac{C_t}{C_t + C_p} \frac{Nk_t}{\gamma_s Z(j\omega)} , \tag{1.32}$$

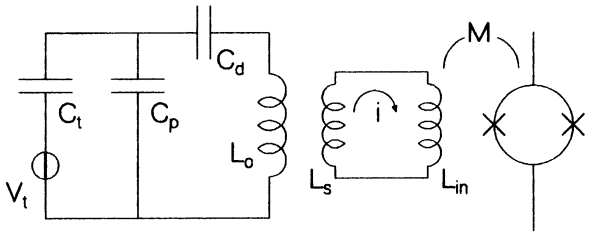

Fig. 3. – Electrical circuit from the transducer to the SQUID. C_t and C_p are the transducer active and parasitic capacitance; C_d is the decoupling capacitance; L_0 is the transformer primary inductance; L_s the secondary inductance; L_{in} is the inductance of the input coil of the SQUID; M is the mutual inductance.

where

$$Z(j\omega) = \frac{1}{j\omega C} + j\omega L_0\left(1 - \frac{k_t^2}{\gamma_s}\right) + R\,, \tag{1.33}$$

with $\gamma_s = (L_s + L_{in})/L_s$, $C = ((C_t + C_p)\,C_d)/(C_t + C_p + C_d)$ and R representing the losses of the electrical circuit. The impedance $Z(j\omega)$ resonates at the angular frequency

$$\omega_{el} = \sqrt{\frac{1}{L_0 C\,(1 - k_t^2/\gamma_s)}}\,, \tag{1.34}$$

which we consider quite larger than the resonances of the mechanical modes ($\nu_{el} \simeq$ 1.8 kHz, $\nu_- \simeq \nu_+ \simeq 900$ Hz). As a consequence, we can assume the impedance $Z(j\omega)$ constant in the frequency range of our interest:

$$Z(j\omega) \sim Z(j\omega_-) \sim Z(j\omega_+) = Z_0\,. \tag{1.35}$$

The SQUID input current is therefore

$$i(t) = \frac{C_t}{C_t + C_p}\,\frac{N k_t v_t(t)}{\gamma_s Z_0}\,, \tag{1.36}$$

where we have neglected the delay introduced by the electrical circuit (the impedance can be assumed constant, but it is not real). The corresponding magnetic flux in the SQUID is given by

$$\phi(t) = M\, i(t) \tag{1.37}$$

and the output voltage of the SQUID amplifier, proportional to the flux, is

$$V(t) = A\phi(t)\,. \tag{1.38}$$

The value of A is evaluated experimentally by means of a known continuous calibration signal at a frequency ν_{cal}, usually chosen between the resonance

frequencies of the two modes, providing

(1.39) $$A = V_{\rm cal}/\phi_{\rm cal},$$

where $\phi_{\rm cal}$ is the applied flux and $V_{\rm cal}$ is the corresponding output.

Overall, we represent the operation of the electrical circuit and of the SQUID amplifier with a constant,

$$V(t)/V_{\rm t}(t) = AB\,,$$

where $B = \phi(t)/V_{\rm t}(t)$ is the proportionality constant between the (unloaded) transducer voltage and the SQUID magnetic flux, given by

(1.40) $$B = \frac{C_{\rm t}}{C_{\rm t} + C_{\rm p}} \frac{N k_{\rm t} M}{\gamma_{\rm s} Z_0}\,.$$

According to the above model, the magnetic flux in the SQUID corresponding to the standard signal eq. (1.22) is

$$\phi_{\rm sig}(t) = \alpha B u_{\rm sig}(t)\,,$$

where $u_{\rm sig}(t)$ is the displacement given by eq. (1.21).

Hence the signal measured at the output of the electronic chain is

(1.41) $$V_{\rm sig}(t) =$$

$$= \alpha AB \sqrt{\frac{2kT_{\rm s}}{m_x}} \frac{1}{(\omega_+^2 - \omega_-^2)} [\omega_+ \exp[-\beta_+ t] \sin\omega_+ t - \omega_- \exp[-\beta_- t] \sin\omega_- t]$$

(where we have introduced $T_{\rm s} = E_{\rm s}/k$).

The r.m.s. magnetic flux in the SQUID due to the narrow-band noise at the two modes, when the tuning condition is fulfilled, is obtained from eq. (1.28)

(1.42) $$\phi_{{\rm br}\pm} = \alpha B \sqrt{\frac{kT_{\rm e}}{2m_y\omega_\pm^2}}$$

and the corresponding r.m.s. output voltage is

(1.43) $$V_{{\rm br}\pm} = \alpha AB \sqrt{\frac{kT_{\rm e}}{2m_y\omega_\pm^2}}\,.$$

In addition to the narrow-band noise we have the noise due to the SQUID and its associated instrumentation, which we assume to have a flat spectrum in the frequency range of our interest. This wide-band noise has spectrum S_ϕ when expressed in terms of magnetic flux in the SQUID, or $S_{\rm n} = S_\phi/B^2$ if referred to the transducer voltage.

Therefore, the total noise spectrum referred at the transducer, using eq. (1.26), is

(1.44) $$S_{\rm t}(\omega) = S_{\rm n} + \alpha^2 S_{fx} |W_{ux}(j\omega)|^2 + \alpha^2 S_{fy} |W_{uy}(j\omega)|^2.$$

We remark that, in addition to this noise, due to known physical effects, we may have some excess noise of non-stationary nature due to possible unknown noise sources.

2. – "Slow" filtering of the data processed by the lock-in amplifiers

We briefly recall here the procedure used to filter the data of the "slow" line, that is the data processed by means of lock-in amplifiers, where the two resonant modes are observed and filtered separately.

If we consider the data after the lock-in amplifiers, at each of the two resonance modes, it is possible to show [6] that the system can be represented with the equivalent model given in fig. 4, where S_{nb} is the narrow-band noise spectrum at the resonance frequency and S_n is the wide-band noise spectrum observed sufficiently far from the two resonance frequencies. $W_1 = \beta_1/(\beta_1 + j\omega)$ represents the transfer function of the mechanical oscillator, as seen through the lock-in amplifier, where β_1 is the dissipation coefficient of the mode (β_- or β_+) and $W_2 = \beta_2/(\beta_2 + j\omega)$ represents the filtering action of the lock-in.

In the absence of signals and of non-Gaussian disturbances the two outputs of the lock-ins, indicated with $x(t)$ and $y(t)$, are Gaussian variables (the noise, both thermal and electronic, has Gaussian distribution with zero mean). We usually consider the quantity

$$r^2(t) = x^2(t) + y^2(t), \tag{2.1}$$

which, under suitable normalization, represents the energy of the antenna's resonant mode. The variable $r^2(t)$ has exponential distribution with mean value T_e [6].

The best estimation of an input short signal, modeled as a delta-function, whose effect is to modify the vibration status of the observed mode, is obtained by using a Wiener filter. This is done by filtering each of the two streams $x(t)$ and $y(t)$ with the transfer function [6]

$$W(j\omega) = \frac{1}{1+\Gamma}\,\frac{1}{W_1 W_2}\,\frac{\beta_3^2}{\beta_3^2 + \omega^2}, \tag{2.2}$$

where

$$\beta_3 \simeq \beta_1/\Gamma^{1/2} \tag{2.3}$$

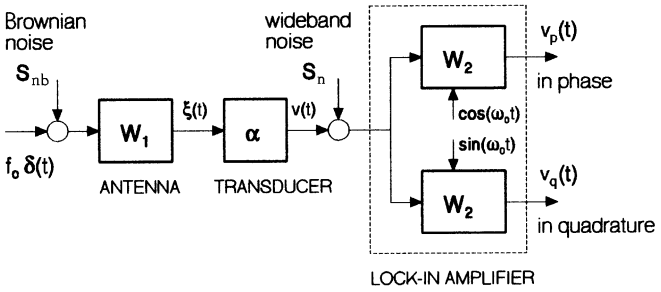

Fig. 4. – Model of antenna, transducer and lock-in amplifier. S_{nb} is the narrow-band noise spectrum at the resonance frequency of the mode and S_n is the wide-band noise spectrum.

defines the overall bandwidth of the detection system (*i.e.* including the filter),

$$\Gamma = \frac{S_{\mathrm{n}}}{S_{\mathrm{nb}}} \tag{2.4}$$

is the spectral ratio at the resonance frequency, typically $\ll 1$ (in the Explorer detector it is of the order of 10^{-7}) and

$$S_{\mathrm{nb}} = V_{\mathrm{br}}^2 / \beta_1, \tag{2.5}$$

with $V_{\mathrm{br}} = V_{\mathrm{br}_\pm}$ given in eq. (1.28). The bandwidth β_3 is much larger than the mechanical bandwidth of the antenna oscillator ($\beta_3 \gg \beta_1$), as can be simply understood noticing that the bar responds in the same way to an excitation due to a g.w. burst and to the Brownian noise and, therefore, the bandwidth of the signal-to-noise ratio is limited only by the noise of the electronic amplifier. The factor $(W_1 W_2)^{-1}$, eq. (2.2), is an inverse filter that cancels the dynamics of the antenna, and $\beta_3^2/(\beta_3^2 + \omega^2)$ is a non-causal smoothing filter, that minimizes the contribution of the wide-band noise.

The filtered data $x_{\mathrm{F}}(t)$ and $y_{\mathrm{F}}(t)$ are squared and summed to obtain the quantity $\varrho^2(t) = x_{\mathrm{F}}(t)^2 + y_{\mathrm{F}}(t)^2$ representing the estimate of the energy innovation of the detector over a time scale of $\simeq 1/\beta_3$. By performing the above operation separately at the two modes, we have two independent estimates $\varrho_-^2(t)$, $\varrho_+^2(t)$ of the input energy innovation which we combine together with the rule

$$\varrho_{\mathrm{min}}^2(t) = \min\left(\varrho_-^2(t), \varrho_+^2(t)\right), \tag{2.6}$$

where each sample of the final sequence is obtained by selecting the minimum value between the two corresponding samples of the mode sequences.

The quantity ϱ_{min}^2, in the absence of signals, has exponential distribution (as ϱ_-^2 and ϱ_+^2). When the filter is normalized so that $\varrho_{\mathrm{min}}^2(0)$ represents the energy (expressed in kelvin) of a short burst applied at $t = 0$, the mean value of the noise distribution of ϱ_{min}^2 is the so called *effective noise temperature* T_{eff}. This quantity expresses the overall sensitivity of the apparatus for pulse detection, as it represents the minimum detectable energy of a burst with signal-to-noise ratio ([4]) equal to 1.

It can be shown that for each mode separately, in the case of perfect tuning ($\Gamma_- = \Gamma_+ = \Gamma$), we have

$$T_{\mathrm{eff}_\pm} \simeq 8\, T_{\mathrm{e}} \sqrt{\Gamma} \tag{2.7}$$

and that the effective temperature of the sequence obtained using the rule (2.6) is given by

$$T_{\mathrm{eff}}^{-1} = T_-^{-1} + T_+^{-1}, \tag{2.8}$$

that is we have

$$T_{\mathrm{eff}} \simeq 4\, T_{\mathrm{e}} \sqrt{\Gamma}\,. \tag{2.9}$$

([4]) Here we consider the ratio between mean-square values. When dealing with data processed by lock-in amplifiers, in fact, the quantities r^2 and ϱ^2 are normalized to represent the mean-square value (energy) of the signal.

The Wiener filter can be realized as discussed above, that is with fixed values of the parameters, or using adaptive techniques, where the parameters are derived from the estimation of the actual noise spectrum of the data and are therefore periodically updated [7, 8].

Another approach to optimum filtering the data processed by the lock-ins consists in applying the theory of the matched filter, which is discussed in the next section. If $S(j\omega)$ is the Fourier transform of the system response to an input burst of a given shape and if $S_t(\omega)$ is the total noise spectrum, then the matched filter transfer function is

$$W_{mf}(j\omega) = K\, S^*(j\omega)/S_t(\omega), \tag{2.10}$$

where K is a constant determined by calibrating the filter using signals of known energy. It is shown in [7] that the matched filter, when aimed at detecting the response to a delta input function, is equivalent to the Wiener filter, in the sense that they have both the same transfer function.

3. – "Fast" filtering using the matched filter

A matched filter [9] aims at detecting a signal of a given shape in the presence of noise and determining its time of occurrence t_0 and its intensity, by maximizing the signal-to-noise ratio. If $o(t)$ is the observation, $n(t)$ the noise and $u(t)$ the known waveform of the signal, then

$$o(t) = n(t) + Au(t - t_0), \tag{3.1}$$

where A and t_0 are unknown constants. For a white noise spectrum the matched filter has impulse response $h(t) = u(-t)$ and transfer function $H(j\omega) = U^*(j\omega)$, where $U(j\omega)$ is the Fourier transform of $u(t)$.

When the spectrum of the noise $S_t(\omega)$ is not white, it is necessary to "whiten" it and then to modify the filter transfer function. Hence, the overall matched filter consists of two sections in cascade: a noise whitening section with transfer function $H_w(j\omega)$ such that $|H_w(j\omega)|^{-2} = S_t(\omega)$, and a proper matched filter section with transfer function $H_p(j\omega) = U^*(j\omega)\cdot H_w^*(j\omega)$. Therefore the overall matched filter transfer function results to be

$$H(j\omega) = \frac{U^*(j\omega)}{S_t(\omega)}. \tag{3.2}$$

From the knowledge of the experimental apparatus it is possible to evaluate the signal response $u(t)$ to an input signal of a given shape. The noise spectrum $S_t(\omega)$ may be derived from a model of the apparatus or it can be estimated from the data. The latter is the "adaptive" realization of the matched filter.

We now consider the application of the matched filter to the data of the resonant gravitational-wave detector considered in the previous sections when sampled directly at relatively high speed, much larger than for the data processed by the lock-in amplifiers. More precisely in what follows we derive the filter matched to the response to a delta-function force applied to the bar oscillator. For simplicity we consider both the signal and the noise referred to the transducer output voltage.

The signal response to $f_x(t) = \delta(t)$ is obtained from (1.22), with Fourier transform $V_t(j\omega) = \alpha W_{ux}(j\omega)$. The expression of the total noise spectrum is given in (1.44). Hence the matched filter transfer function is

$$H(j\omega) = \frac{\alpha W_{ux}^*}{S_n + \alpha^2 S_{fx} |W_{ux}|^2 + \alpha^2 S_{fy} |W_{uy}|^2}, \tag{3.3}$$

which we write as follows:

$$H(j\omega) = \frac{1}{\alpha W_{ux}} \frac{\alpha^2 |W_{ux}|^2}{S_n + \alpha^2 S_{fx} |W_{ux}|^2 + \alpha^2 S_{fy} |W_{uy}|^2}. \tag{3.4}$$

This function represents the cascade of two filters: an *inverse filter*, $1/(\alpha W_{ux})$, that cancels the dynamics of the antenna and of the transducer, and a *smoothing filter*, that limits the bandwidth as required to reduce the wide-band noise contribution.

3˙1. *Response to the signal.* – In the following we shall study the matched filter response to a delta input force applied to the bar. We derive the time domain expression of the filtered signal, and find a *spectral ratio* parameter, similar to the Γ parameter of the Wiener filter applied to the "slow" data, in order to compare the characteristics of the two filters.

Since the signal applied to the matched filter is $\alpha W_{ux}(j\omega)$, the corresponding output is $\alpha^2 G(\omega)$, where

$$G(\omega) = |W_{ux}(j\omega)|^2 / S_t(\omega) \tag{3.5}$$

is the transfer function of the smoothing filter section. The filtered signal, neglecting the scale factor α^2, is therefore the inverse Fourier transform of $G(\omega)$.

The function

$$G(\omega) = \frac{\mu^2 \omega^4}{\mu^2 \omega^4 \alpha^2 S_{fx} + S_n m_y^2 |D(j\omega)|^2 + \alpha^2 S_{fy} | - \omega^2 + 2j\omega\beta_x + \omega_x^2 |^2} \tag{3.6}$$

can be written, by introducing the variable $y = \omega^2$, as

$$G_y(y) = \frac{\mu^2 y^2}{y^4 L + y^3 M + y^2 N + yO + P}, \tag{3.7}$$

with

$$\begin{cases} L = S_n m_y^2; \qquad M = S_n m_y^2 (2B + A^2), \\ N = \mu^2 \alpha^2 S_{fx} + S_n m_y^2 (2\omega_+^2 \omega_-^2 + B^2 - 2AC) + \alpha^2 S_{fy}, \\ O = S_n m_y^2 (2B\omega_+^2 \omega_-^2 + C) + \alpha^2 S_{fy} (4\beta_x^2 - 2\omega_x^2), \\ P = \alpha^2 S_{fy} \omega_x^4 + S_n m_y^2 \omega_+^4 \omega_-^4 \end{cases} \tag{3.8}$$

and A, B, C given by eq. (1.9). The poles of G_y have been obtained by solving the quartic equation using the software package *Macsyma*:

$$y_1 = \omega_1^2 = a + jb\,; \qquad y_2 = \omega_2^2 = a - jb\,,$$

$$y_3 = \omega_3^2 = c + jd\,; \qquad y_4 = \omega_4^2 = c - jd\,,$$

where $|b| \ll |a|$, $|d| \ll |c|$, $b, d \leqslant 0$.

In terms of ω, we have the following eight roots:

$$\omega_1 = \sqrt{a + jb}\,, \qquad -\omega_1 = -\sqrt{a + jb}\,,$$

$$\omega_2 = \sqrt{a - jb}\,, \qquad -\omega_2 = -\sqrt{a - jb}\,,$$

$$\omega_3 = \sqrt{c + jd}\,, \qquad -\omega_3 = -\sqrt{c + jd}\,,$$

$$\omega_4 = \sqrt{c - jd}, \qquad -\omega_4 = -\sqrt{c - jd}.$$

The real parts of the roots are

$$a = -(M/4L) + (\Delta_{12}/2) \simeq \omega_+^2\,, \tag{3.9}$$

$$c = -(M/4L) - (\Delta_{12}/2) \simeq \omega_-^2\,, \tag{3.10}$$

where M and L are given in eqs. (3.8), $\Delta_{12} = \omega_+^2 - \omega_-^2$, and the approximation is obtained by neglecting terms with $\beta_\pm^2$ with respect to $\omega_{1,2}^2$.

The imaginary parts of the roots will be considered at the end of this section.

The inverse Fourier transform of $G(\omega)$ is

$$g(t) = \frac{1}{(2\pi S_n m_x^2)} \int_{-\infty}^{\infty} \frac{\omega^4 \exp[j\omega t]}{(\omega^2 - \omega_1^2)(\omega^2 - \omega_2^2)(\omega^2 - \omega_3^2)(\omega^2 - \omega_4^2)}\,\mathrm{d}\omega = \tag{3.11}$$

$$= \frac{1}{(2\pi S_n m_x^2)}\, 2\pi j \sum \text{res}\,.$$

By evaluating this integral in its region of convergence, that is considering the poles

$$-\omega_1 = -a' - jb'\,, \qquad \omega_2 = a' - jb'\,, \qquad -\omega_3 = -c' - jd'\,, \qquad \omega_4 = c' - jd'\,,$$

we obtain the result

$$g(t) = \tag{3.12}$$

$$= j\left[\frac{(-\omega_1)^4 \exp[b't]\exp[-ja't]}{2\omega_1(\omega_1^2-\omega_2^2)(\omega_1^2-\omega_3^2)(\omega_1^2-\omega_4^2)} + \frac{\omega_2^4 \exp[b't]\exp[ja't]}{2\omega_2(\omega_2^2-\omega_1^2)(\omega_2^2-\omega_3^2)(\omega_2^2-\omega_4^2)}\right]\Big/(S_n m_x^2) +$$

$$+ j\left[\frac{(-\omega_3)^4 \exp[d't]\exp[-jc't]}{2\omega_3(\omega_3^2-\omega_1^2)(\omega_3^2-\omega_2^2)(\omega_3^2-\omega_4^2)} + \frac{\omega_4^4 \exp[d't]\exp[jc't]}{2\omega_4(\omega_4^2-\omega_1^2)(\omega_4^2-\omega_2^2)(\omega_4^2-\omega_3^2)}\right]\Big/(S_n m_x^2),$$

that can be expressed as the following sum of two oscillating terms with two-sided

exponential decay

$$g(t) = \frac{\exp[b'|t|]}{4\omega_+ S_n m_x^2 b' |(\omega_1^2-\omega_3^2)(\omega_1^2-\omega_4^2)|^2}[\zeta_1\cos(\omega_+ t)+\zeta_2\sin(\omega_+ t)] +$$

$$+ \frac{\exp[d'|t|]}{4\omega_- S_n m_x^2 d' |(\omega_3^2-\omega_1^2)(\omega_3^2-\omega_2^2)|^2}[\eta_1\cos(\omega_- t)+\eta_2\sin(\omega_- t)],$$

where

$$\omega_1^3\overline{(\omega_1^2-\omega_3^2)(\omega_1^2-\omega_4^2)} = \zeta_1 - j\zeta_2$$

(the overline bar indicates the complex conjugation) and

$$\omega_3^3\overline{(\omega_3^2-\omega_1^2)(\omega_3^2-\omega_2^2)} = \eta_1 - j\eta_2.$$

This can be simplified as follows under the high-Q approximation, that is by considering that b, d are both much smaller than a, c:

$$g(t) \simeq \frac{\omega_+^2 \exp[b'|t|]}{4b' S_n m_x^2(\omega_+^2-\omega_-^2)^2}\cos(\omega_+ t) + \frac{\omega_-^2 \exp[d'|t|]}{4d' S_n m_x^2(\omega_+^2-\omega_-^2)^2}\cos(\omega_- t) \tag{3.13}$$

that in the tuning condition (see eq. (1.14)) becomes

$$g(t) \simeq \frac{\exp[b'|t|]}{16\mu b' S_n m_x^2 \omega_0^2}\cos(\omega_+ t) + \frac{\exp[d'|t|]}{16\mu d' S_n m_x^2 \omega_0^2}\cos(\omega_- t). \tag{3.14}$$

Here the parameters b' and d' (expressed in rad/s) represent the inverse of the decay times of the impulse response at the modes. In appendix A we derive their expressions and we show that, in the tuning condition,

$$|b'| \simeq (1/2)\,\omega_+\beta_+^2/(\omega_+^2\sqrt{\Gamma_{3+}}) \simeq \beta_+/\sqrt{\Gamma_+}, \tag{3.15}$$

$$|d'| \simeq (1/2)\omega_-\beta_-^2/(\omega_-^2\sqrt{\Gamma_{3-}}) \simeq \beta_-/\sqrt{\Gamma_-}, \tag{3.16}$$

where

$$\Gamma_\pm = S_n/S_{nb_\pm}$$

are the spectral ratios between the wide-band and the narrow-band noise spectra, which we introduced in sect. **2**, and

$$\Gamma_{3+} \simeq \Gamma_+\beta_+^2/(4\omega_+^2) = \Gamma_+/(16Q_+^2), \tag{3.17}$$

$$\Gamma_{3-} \simeq \Gamma_-\beta_-^2/(4\omega_-^2) = \Gamma_-/(16Q_-^2). \tag{3.18}$$

As a conclusion, the decay times of the optimum filter response to an input burst signal are the same if we consider data processed by means of lock-in amplifiers or data directly sampled, since from eqs. (3.15), (3.16) and (2.3) we have

$$|b'| \simeq \beta_{3+}, \qquad |d'| \simeq \beta_{3-}. \tag{3.19}$$

The impulse response $g(t)$, given by (3.13) or (3.14), only exhibits an overall exponential decay if $b' = d'$ (very tight coupling of the oscillators, with $\beta_- \simeq \beta_+$). In the general case with $b' \neq d'$ we have two time constants: the smallest dominating at short times, the largest at long times.

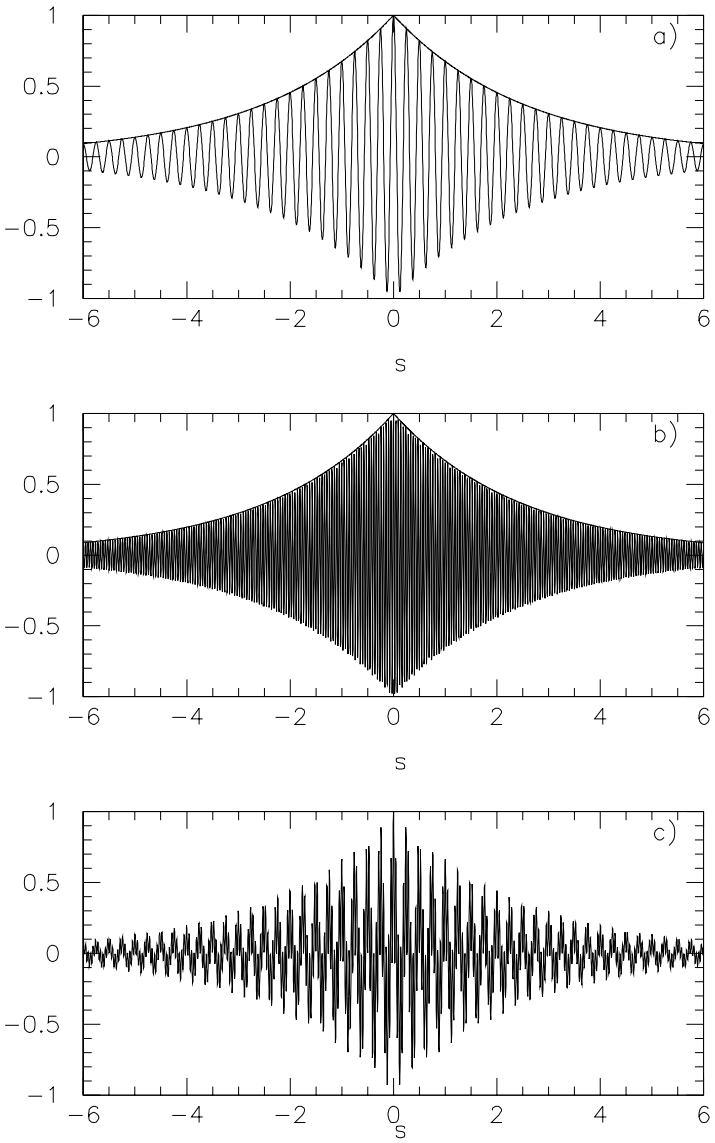

Fig. 5. – Normalized matched filter response to a delta input signal and envelope of its modulus. *a*) at ν_-, with $|d'| = 0.4$ rad s^{-1} (the oscillation is at the aliased frequency $\nu_- \simeq 4$ Hz); *b*) at ν_+, with $|b'| = 0.4$ rad s^{-1} (the oscillation is at the aliased frequency $\nu_+ \simeq 25$ Hz); *c*) overall response with $|d'| = |b'| = 0.4$ rad s^{-1} (the beating is due to the sum of the oscillations at the two aliased resonance frequencies).

In fig. 5 we plot the functions

$$g_-(t) = \frac{\omega_-^2 \exp[d'|t|]}{4d'(\omega_+^2 - \omega_-^2)^2} \cos(\omega'_- t), \qquad g_+(t) = \frac{\omega_+^2 \exp[b'|t|]}{4b'(\omega_+^2 - \omega_-^2)^2} \cos(\omega'_+ t),$$

$$g(t) = g_-(t) + g_+(t)$$

that represent, respectively, the impulse response at ν_-, at ν_+ and the overall response, for the particular case of equal values of the parameters b' and d' ($d' = b' = 0.4$ rad/s). In fig. 6 we plot the same functions for the case $d' = 4$ rad/s and $b' = 2$ rad/s.

Note that the angular frequencies involved in the above are not the actual frequencies, but the corresponding aliased angular frequencies $\omega'_+ = 2\pi(921 - 900)$ rad/s; $\omega'_- = 2\pi(904 - 900)$ rad/s , as we would find by filtering the data with the actual data acquisition systems of our detectors (see sect. **4**).

We have shown that the basic parameters which describe the impulse response of an optimum filter are the same for both the "fast" and the "slow" filtering procedures. The basic difference is that the response of the "fast" filter is oscillating while that of the "slow" filter is not.

More precisely, when considering the impulse response of the two filters, separately at the two modes, we find that the response of the "slow" filter is the envelope of the modulus of the corresponding response of the "fast" filter, as shown by the plots of fig. 7. The oscillating nature of the direct response permits to obtain, for large SNRs, a higher temporal resolution, that is to determine the arrival time of the input burst signal with a precision of the order of $1/\nu'_-$, $1/\nu'_+$ respectively for the two modes, where ν'_- and ν'_+ are the aliased resonance frequencies. This resolution for the overall response, that is the sum of two oscillations at ν'_- and ν'_+, is $\simeq 1/\nu'_+$ (see fig. 5*c*) and 6*c*)).

3'2. *Response to the noise and effective temperature.* – We consider here the noise response of the matched filter with reference to the block diagram of fig. 8, where we represent the noise process at the transducer, with spectrum $S_t(\omega)$ given by eq. (1.44), as generated by a system with transfer function $N(j\omega)$ driven by a white-noise source with unit spectrum ($S_0 = 1$).

This means that $|N(j\omega)|^2 = S_t(\omega)$. The filtered noise spectrum is therefore

$$S_m(\omega) = S_t(\omega) \cdot |W_{ux}(j\omega)|^2 / |N(j\omega)|^4 \tag{3.20}$$

that is, using (3.5)

$$S_m(\omega) = G(\omega). \tag{3.21}$$

The inverse Fourier transform of this function gives the autocorrelation of the noise at the filter output, whose value at zero delay represents the filtered noise variance

$$\sigma_m^2 = (1/2\pi) \int_{-\infty}^{+\infty} G(\omega)\, d\omega . \tag{3.22}$$

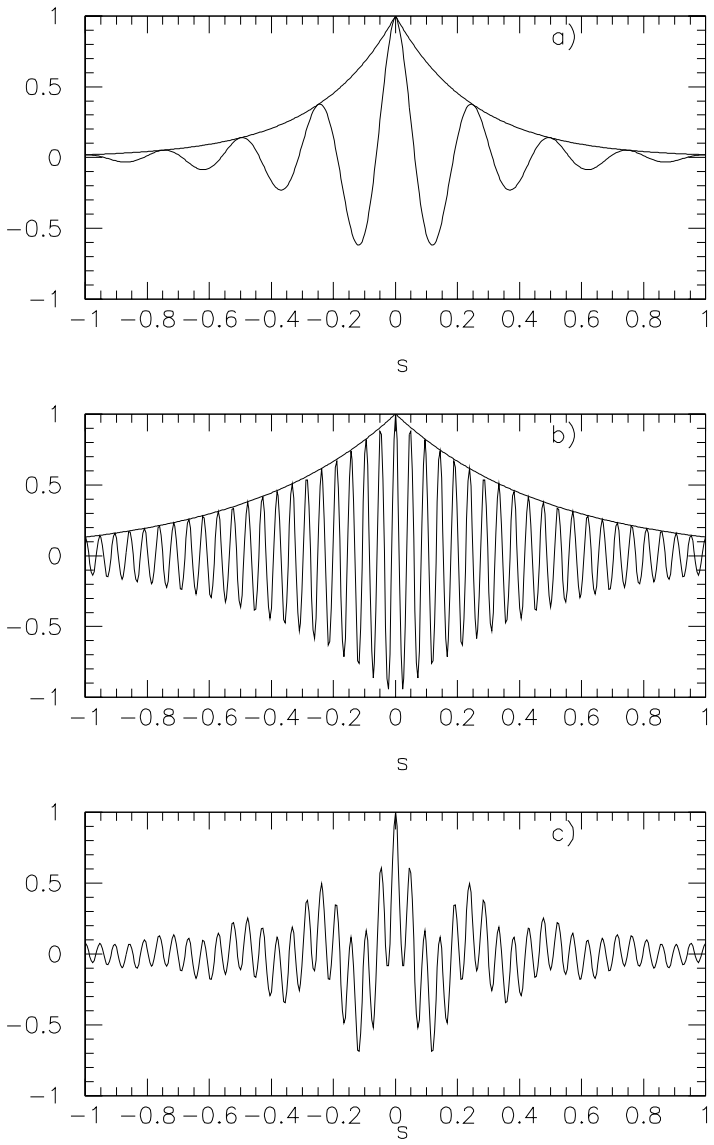

Fig. 6. – *a*) Same as fig. 5*a*), with $|d'| = 4$ rad s^{-1}; *b*) same as fig. 5*b*), with $|d'| = 2$ rad s^{-1}; *c*) Same as fig. 5*c*), with $|d'| = 4$ rad s^{-1}, $|b'| = 2$ rad s^{-1}: here the envelope is not a simple exponential.

Therefore both the noise variance and the maximum value $g(0)$ of the filtered signal are determined by the same quantity

$$\sigma_{\mathrm{m}}^2 = g(0) = (1/2\pi) \int_{-\infty}^{+\infty} G(\omega)\, \mathrm{d}\omega = R_0. \tag{3.23}$$

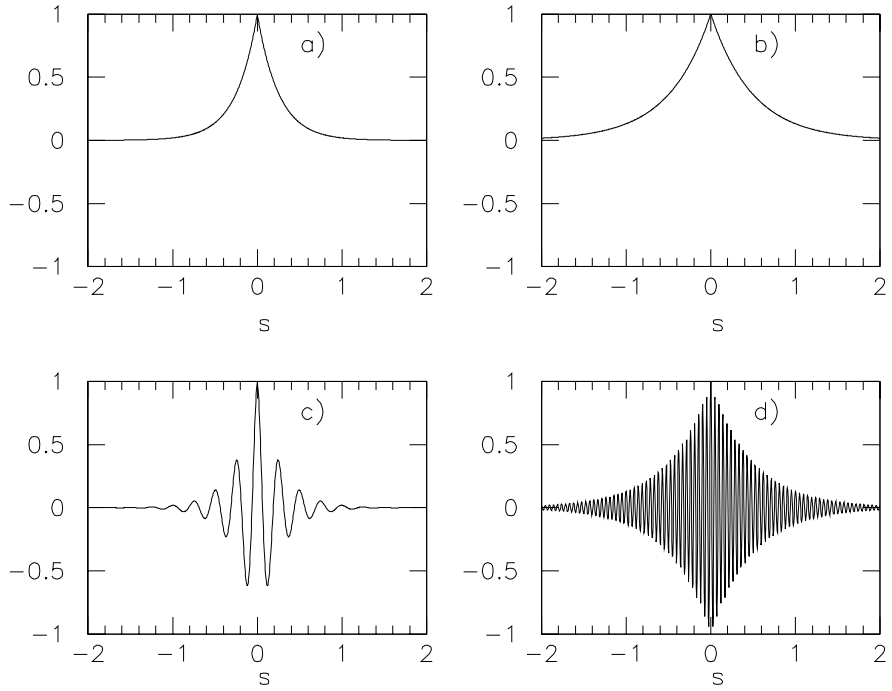

Fig. 7. – The Wiener filter ("slow" data) response to a delta input signal (*a*) and *b*)) is the envelope of the matched filter ("fast" data) response to the same signal (*c*) and *d*)). We have used the same parameters in both cases: $\Gamma_- = 6.2 \cdot 10^{-10}$, $\Gamma_+ = 2.5 \cdot 10^{-9}$; $\beta_{3-} = 4$ rad/s, $\beta_{3+} = 2$ rad/s; $|d|' = 4$ rad/s, $|b|' = 2$ rad/s.

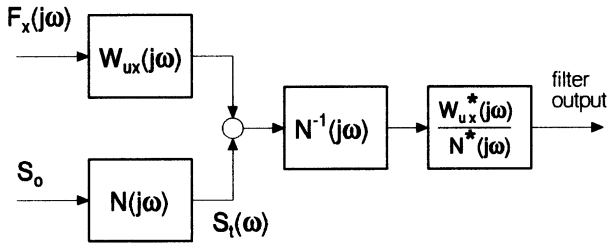

Fig. 8. – Block diagram of the antenna and matched filter chain. $N(j\omega)$ is such that $|N(j\omega)|^2 = S_t(\omega)$ (the white noise at the input of $N(j\omega)$ is $S_0 = 1$, with $S_t(\omega) = S_0 |N(j\omega)|^2$). $F_x(j\omega)$ is the Fourier transform of the input force.

Also the signal-to-noise ratio after the matched filter

$$(\mathrm{SNR})_m = g(0)^2 / \sigma_m^2 = R_0 \tag{3.24}$$

is expressed by the same quantity R_0, which only depends on the transfer function $G(\omega)$ of the smoothing filter.

As a consequence, the function $G(\omega)$, which we shall refer to as the filter spectral

gain in the following, assumes the meaning of spectral distribution of the signal-to-noise ratio, thereby providing indications for the choice of the actual observation bandwidth of the data acquisition instrumentation. Moreover, the widths of the peaks of the function $G(\omega)$ at the two modes, that are $|b'|$ and $|d'|$, respectively, assume the meaning of SNR bandwidths. For the tuned case we have from eq. (3.19)

$$\Delta\nu_- \simeq \beta_{3_-}/\pi\,, \qquad \Delta\nu_+ \simeq \beta_{3_+}/\pi\,. \tag{3.25}$$

Let us consider now the tuned case for tight coupling between the oscillators, that is with $\beta_- = \beta_+ = \beta_1$, $S_{\mathrm{nb}_-} = S_{\mathrm{nb}_+} = S_{\mathrm{nb}}$, $\Gamma_- = \Gamma_+ = \Gamma$.

From eq. (3.14) we have

$$R_0 = 1/(S_{\mathrm{n}} m_x^2)\left(\frac{1}{16\mu|b|'\omega_0^2} + \frac{1}{16\mu|d|'\omega_0^2}\right). \tag{3.26}$$

Being $|b|' = |d|' = \beta_1/\sqrt{\Gamma}$, the signal-to-noise ratio for a burst with $f_0\tau = 1$ is

$$R_0 = 1\ /(\sqrt{\Gamma}\, S_{\mathrm{nb}}\beta_1 m_x^2 8\mu\omega_0^2) \tag{3.27}$$

that is, being $\sigma_{\mathrm{nb}}^2 = 2V_{\mathrm{br}}^2$ from eq. (1.30) and $S_{\mathrm{nb}} = V_{\mathrm{br}}/\beta_1$ from eq. (2.5),

$$R_0 = 1\ /(4\sqrt{\Gamma}\,\sigma_{\mathrm{nb}}^2\mu m_x^2\omega_0^2)\,. \tag{3.28}$$

For a burst of energy $E_{\mathrm{s}} = kT_{\mathrm{s}}$, that is with $f_0\tau = \sqrt{2kT_{\mathrm{s}}m_x}$, we have

$$(\mathrm{SNR})_{\mathrm{m}} = 2kT_{\mathrm{s}}m_x R_0 = T_{\mathrm{s}}/(2\sqrt{\Gamma T_{\mathrm{e}}})\,. \tag{3.29}$$

In order to evaluate the SNR improvement introduced by the filter, we compare the signal-to-noise ratio provided by the filter with that obtained without filtering the data, that we derived in subsect. **1**·3 and repeat here for convenience:

$$(\mathrm{SNR})_0 = 2T_{\mathrm{s}}/T_{\mathrm{e}}. \tag{3.30}$$

Finally the ratio of the two signal-to-noise ratios is

$$(\mathrm{SNR})_{\mathrm{m}}/(\mathrm{SNR})_0 = 1/(4\sqrt{\Gamma})\,. \tag{3.31}$$

This SNR improvement introduced by the filter can be expressed in terms of a reduction of the temperature of the noise from the equivalent temperature T_{e} to the effective temperature T_{eff}. Having $(\mathrm{SNR})_{\mathrm{m}}/(\mathrm{SNR})_0 = T_{\mathrm{e}}/T_{\mathrm{eff}}$, we obtain

$$T_{\mathrm{eff}} = 4T_{\mathrm{e}}\sqrt{\Gamma}\,, \tag{3.32}$$

that is in full agreement with the result (2.9), obtained for the "slow" filtering procedure.

There is, however, an important difference between the two procedures. When we consider, as usual, the maximum of the response to a signal burst of energy kT_{s}, the output of the slow filter is kT_{s} (as it behaves as an r.m.s. detector) and the noise is kT_{eff}; while that of the fast filter is $2kT_{\mathrm{s}}$ (as it behaves as a peak detector) and the noise is again kT_{eff}.

As a consequence, if we normalize the energy scale to the peak value of the signal, the noise of the "fast" filter is $kT_{\mathrm{eff}}/2$, which we assume as the "apparent" effective temperature of this filter. For the "fast" filter, in other words, we have an improvement

of the signal-to-noise ratio for pulse detection of a factor of two in comparison with the "slow" filter.

3·3. *The distribution of the filtered data.* – We consider here the distribution of the filtered data, as it significantly affects the detection probability of a signal of given intensity or of given signal-to-noise ratio.

For the slow filtering procedure, applied to the data processed by lock-in amplifiers, we consider the variable $\varrho^2 = x_{\mathrm{F}}^2 + y_{\mathrm{F}}^2$ (see sect. **2**). Since x_{F} and y_{F} are zero mean normal variables, in the absence of signals the probability density function of ϱ^2 is exponential:

$$f_{\mathrm{w}}(\varrho^2) = \frac{1}{\sigma_{\mathrm{w}}^2} \exp\left[\frac{-\varrho^2}{\sigma_{\mathrm{w}}^2}\right], \tag{3.33}$$

with

$$E[\varrho^2] = \sigma_{\mathrm{w}}^2 .$$

For the fast-filtering procedure we consider the variable g_{m}^2, where g_{m} is the output of the matched filter, that is, in the absence of signals, a zero mean variable with variance σ_{m}^2. But if we represent with g_{m}^2 the energy of the signal, the variance of the noise is $\sigma_{\mathrm{m}}^2/2$. With this normalization the probability density function is therefore

$$f_{\mathrm{m}}(g_{\mathrm{m}}^2) = \frac{1}{\sigma_{\mathrm{m}}\sqrt{\pi g_{\mathrm{m}}^2}} \exp\left[\frac{-g_{\mathrm{m}}^2}{\sigma_{\mathrm{m}}^2}\right], \tag{3.34}$$

with

$$E[g_{\mathrm{m}}^2] = \sigma_{\mathrm{m}}^2/2 .$$

In order to compare the two distributions, we now express the probability density functions in terms of variables normalized to their expected value, that is in terms of signal-to-noise ratios. With $V_{\mathrm{w}} = \varrho_{\mathrm{w}}^2/\sigma_{\mathrm{w}}^2$ eq. (3.33) becomes

$$f_{\mathrm{w}}(V_{\mathrm{w}}) = \exp[-V_{\mathrm{w}}] . \tag{3.35}$$

With $V_{\mathrm{m}} = g_{\mathrm{m}}^2/\sigma_{\mathrm{m}}^2$, eq. (3.34) becomes

$$f_{\mathrm{m}}(V_{\mathrm{m}}) = \frac{1}{\sqrt{\pi V_{\mathrm{m}}}} \exp[-V_{\mathrm{m}}] . \tag{3.36}$$

Now we consider the functions

$$P_{\mathrm{w}}(V_{\mathrm{w}}) = \int_{V_{\mathrm{w}}}^{\infty} f_{\mathrm{w}}(V')\,\mathrm{d}V' = \exp[-V_{\mathrm{w}}], \tag{3.37}$$

$$P_{\mathrm{m}}(V_{\mathrm{m}}) = \int_{V_{\mathrm{m}}}^{\infty} f_{\mathrm{m}}(V')\,\mathrm{d}V' = 1 - \mathrm{erf}(\sqrt{V_{\mathrm{m}}}) \tag{3.38}$$

that represent the probability to have, by chance, a value of noise greater than

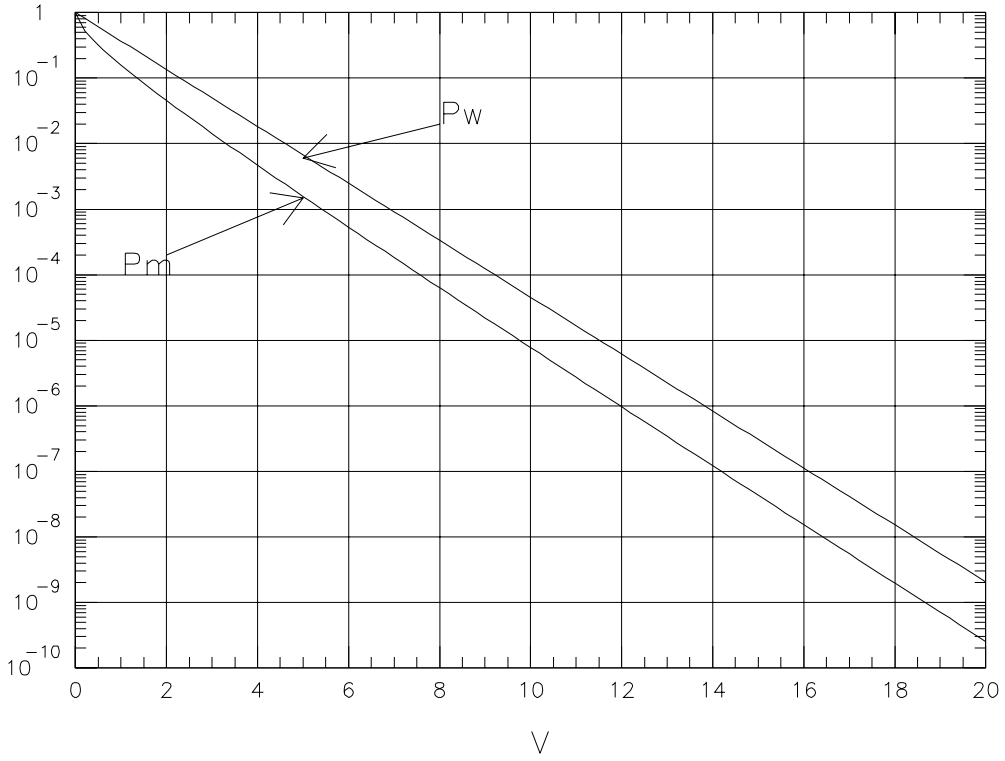

Fig. 9. – Probability to have by chance a sample with signal-to-noise ratio above the threshold V for the "fast" ($P_{\rm m}$) and the "slow" ($P_{\rm w}$) filtered data.

a fixed value and hence the probability that a sample with SNR greater than a given threshold $V_{\rm m}$ is due to the noise.

$P_{\rm w}(V_{\rm w})$ and $P_{\rm m}(V_{\rm m})$ are plotted in fig. 9: we can see that the probability to have, by chance, a sample with SNR greater than a fixed value of threshold $V = V_{\rm m} = V_{\rm w}$ is always smaller for the "fast" data. This means that the fast data provide a better safety margin in identifying a sample above threshold as a candidate gravitational signal.

Now let us consider the ratio between the two probabilities for equal values of the SNR, that is with $V = V_{\rm m} = V_{\rm w}$:

$$G_P(V) = \frac{P_{\rm w}(V)}{P_{\rm m}(V)} .$$

This ratio represents the probability gain of the "fast" with respect to the "slow" filter. As shown in fig. 10*a*), $P_{\rm w}(V)/P_{\rm m}(V)$, always greater than or equal to 1, increases as the SNR.

From a different viewpoint, we can express the improvement of performance provided by the "fast" filter in terms of an effective temperature gain G_T for a given detection probability value. A given value of $P = P_{\rm w} = P_{\rm m}$ is in fact obtained with a smaller SNR for the "fast" filter than for the "slow" filter.

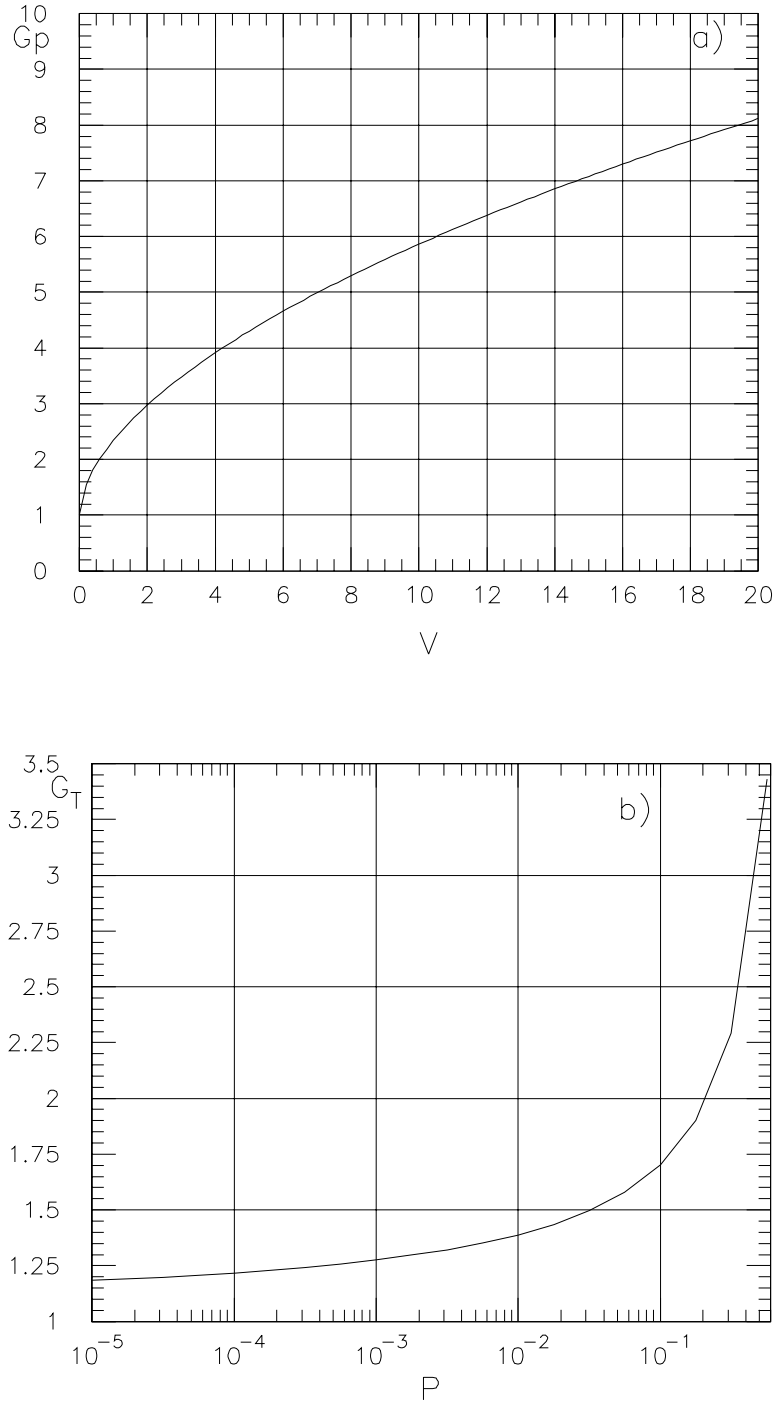

Fig. 10. – *a*) Probability gain $G_P = P_w/P_m$ *vs.* the SNR V; *b*) Temperature gain G_T of the "fast" filtering procedure with respect to the "slow" filtering procedure as a function of the probability P.

From the condition

$$P_{\mathrm{w}}(V_{\mathrm{w}}^*) = P_{\mathrm{m}}(V_{\mathrm{m}}^*)$$

we derive the ratio $G_T = V_{\mathrm{w}}^*/V_{\mathrm{m}}^*$ which represents the SNR gain. This quantity is plotted in fig. 10*b*) as a function of the probability P.

4. – Data acquisition and storage: bandwidth and sampling

The detector output signal contains useful information, as contributing to the overall signal-to-noise ratio, in the frequency range where the spectral gain $G(\omega)$ is not vanishing. Most of the contribution usually comes from ranges of a few hertz near the resonance frequencies of the two modes, defined by the SNR bandwidths (3.25).

When dealing with the Explorer detector (see table II, in subsect. **4**·1) we consider of our interest a frequency range of the order of 27.5 Hz, which includes both the resonances of the system. The actual bandwidth of the signal is determined by filtering it, before sampling, with a six-pole bandpass filter with flat response between 902 and 926 Hz and strong attenuation outside.

According to the Nyquist theorem, the minimum sampling frequency, which allows the original analog signal to be exactly reconstructed from its samples, is twice the bandwidth, not twice the maximum frequency, of the signal. Then we may sample the data at a rate that depends only on the observation bandwidth of our interest.

We have chosen to sample the data at 220 Hz [10]. As a consequence, the frequency region between 900 and 927.5 Hz is transposed in the range 20–47.5 Hz as obtained by subtracting 880 Hz from the above values. The overall bandwidth of the sampled signal is from 0 to 110 Hz, corresponding to 880–990 Hz for the original data.

The signal sampled at 220 Hz is then processed in software, before the final storage, *i.e.* it is subsampled by a factor of four in order to minimize the amount of data by storing only the information required to cover the range between 900 and 927.5 Hz.

This subsampling is performed in the frequency domain: every $N = 16384$ samples we perform the fast Fourier transform on the data. Then we select only the samples in the frequency range 900–927.5 Hz and on these data, $1/4$ of the total, we perform the inverse Fourier transform (in practice, because the Fourier transform is and must remain symmetrical, we select the $N/8$ data in the range 900–927.5 and the $N/8$ data in the range 1052.5–1080 and we concatenate these two sequences before performing the inverse Fourier transform).

The final sampling time of the data, as they are stored, is therefore 18.18 ms. We remark, however, that from them we can reconstruct the signal sampled at 4.54 ms, by performing the Fourier transform, adding data of value zero (we know that the signal spectrum outside the 900–927.5 range is only due to noise) and then by antitransforming.

The data processed by means of lock-in amplifiers are subsampled by a factor 64 with respect to those sampled at 4.54 ms.

Table I reports the exact values of the sampling rates and of the initial frequencies in the data sets.

As done in the previous section, we will refer to the data processed with lock-ins as to the “slow data” and to the data sampled at 4.54 ms as to the “fast data”.

TABLE I. – *Explorer detector.*

Sampling rate $\Delta\nu_{ff}$	220.07042 Hz
(Sampling time Δt_{ff}	4.544 ms)
Sampling rate $\Delta\nu_{f}$	55.0176 Hz
(Sampling time Δt_{f}	18.176 ms)
Sampling rate $\Delta\nu_{s}$	3.43860 Hz
(Sampling time Δt_{s}	290.0816 ms)
Initial frequency, data @ $\Delta\nu_{ff}$	880.281677 Hz
Initial frequency, data @ $\Delta\nu_{f}$	900.026770 Hz

TABLE II. – *Explorer*.

	1991	1994
Mass of the bar (kg)	2270	—
Bar length L (m)	3	—
Equivalent mass of the transducer m_y (kg)	0.346	0.304
Gap of the transducer d (μm)	52	63.4
Transducer bias voltage V_b (V)	320	165
Bar temperature T_{bar} (K)	2.9	2.4
Frequency of the mode ν_- (Hz)	904.7	907.05
Frequency of the mode ν_+ (Hz)	921.3	923.26
Decay time $1/\beta_-$ of the mode ν_- (s)	270	1400
Decay time $1/\beta_+$ of the mode ν_+ (s)	350	2000
SNR bandwidth $\Delta\nu_-$ (Hz)	1.55	0.14
SNR bandwidth $\Delta\nu_+$ (Hz)	0.98	0.13
Γ_-	$5.7\cdot10^{-7}$	$2.5\cdot10^{-6}$
Γ_+	$8.5\cdot10^{-7}$	$1.4\cdot10^{-6}$
Brownian flux of the mode $\nu_-(T=1\ \mathrm{K})$ (ϕ_0)	$8.3\cdot10^{-5}$	$1.8\cdot10^{-5}$
Brownian flux of the mode $\nu_+(T=1\ \mathrm{K})$ (ϕ_0)	$6.0\cdot10^{-5}$	$2.0\cdot10^{-5}$

4·1. *The Explorer detector.* – The characteristics of the experimental apparatus during the 1991 and 1994 runs are shown in table II. One of the main differences between the two runs is the value of the Q factors, that in 1994 were about five times larger than in 1991.

Figure 11*a*) shows a power spectrum obtained with two hours of data of the Explorer detector during November 1991 in the frequency range 0–27.5 Hz, representing the range 900–927.5 Hz. In the graph it is possible to observe the two resonances at $\nu_- - 900 = 4.7$ Hz and at $\nu_+ - 900 = 21.3$ Hz, and the peak due to the calibration signal at $\nu_{cal} - 900 = 13.0$ Hz. The wide-band noise level is of the order of $2\cdot10^{-6}\phi_0/\sqrt{\mathrm{Hz}}$ (we recall that the flux quantum is $\phi_0 = 2.07\cdot10^{-15}$ Wb). The variance of the Brownian resonant noise is $\simeq(10^{-4}\phi_0)^2$ for the plus mode and $\simeq(1.4\cdot10^{-4}\phi_0)^2$ for the minus mode.

Figure 11*b*) shows a power spectrum obtained with two hours of data of the Explorer detector during April 1994. The two resonance frequencies are at $\nu_- - 900 = 7.0$ Hz and at $\nu_+ - 900 = 23.2$ Hz and the peak due to the calibration signal at $\nu_{cal} - 900 = 14.5$ Hz. The variance of the Brownian resonant noise is $\simeq(3\cdot10^{-5}\phi_0)^2$,

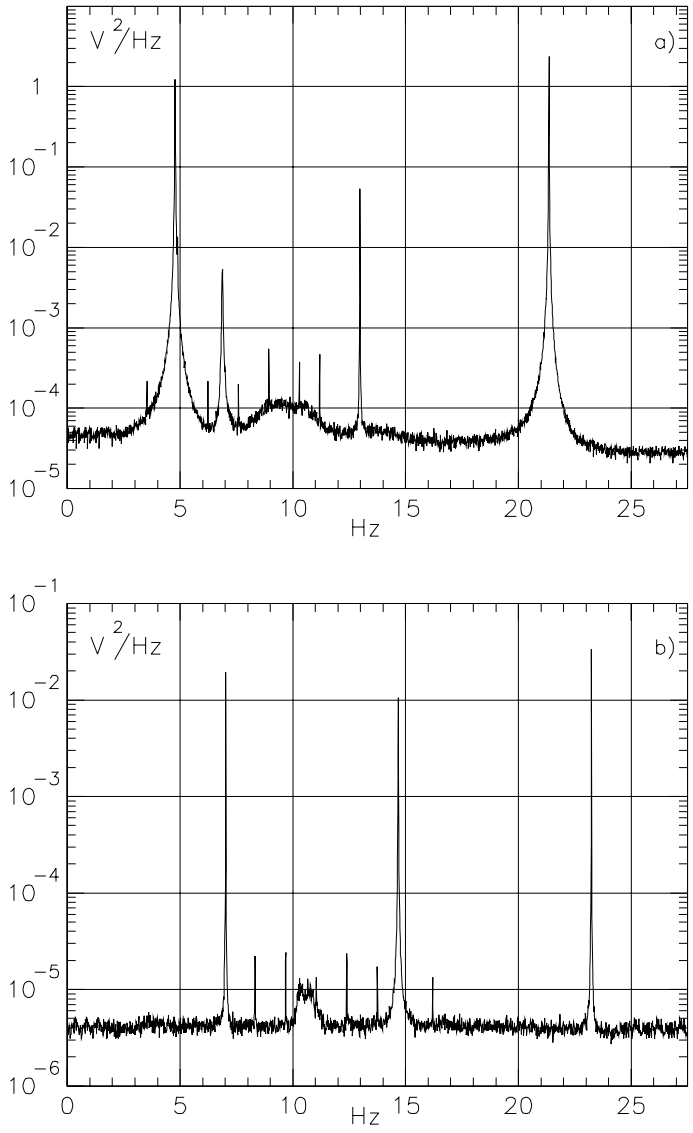

Fig. 11. – Power spectrum obtained with two hours of Explorer data. The initial frequency is 900.02 Hz. *a*) during November 1991; *b*) during April 1994.

for both the resonances, and the wide-band noise level is of the order of $1.6 \cdot 10^{-6} \phi_0 / \sqrt{\text{Hz}}$.

4·2. *Spectral parameter estimation.* – In order to construct the matched filter, it is necessary to know the values of the two resonance frequencies and of the two decay times of the system (in the next paragraph we shall discuss the precision we need). To get this information it is necessary to determine a spectrum with high-frequency resolution.

We perform a new spectral estimation every 2 hours, by averaging 12 different periodograms to reduce the variance of the estimation. This is the result of a compromise between the necessity of using a long period of time to obtain high resolution and the problems of the non-stationarity in the data. Each periodogram is performed on 32768 samples (corresponding to the observation time $T = 595.59$ s with sampling time $\Delta t_f = 18.176$ ms) thus obtaining a frequency resolution of $\delta\nu_h = 1.68 \cdot \cdot 10^{-3}$ Hz.

The algorithm used for estimating the resonance frequencies is based on the Lorentzian behaviour of the theoretical power spectrum around each one of the two resonance frequencies

$$L(\omega) = \frac{1}{(\omega^2 - \omega_i^2)^2 + 4\beta_i^2\omega^2}, \tag{4.1}$$

where ω_i indicates ω_- or ω_+, β_i indicates β_- or β_+. Putting $x = \omega^2$ in the above, we consider

$$y(x) = \frac{1}{L(x)} = x^2 + 2x(2\beta_i^2 - \omega_i^2) + \omega_i^4 = ax^2 + bx + c, \tag{4.2}$$

where

$$a = 1, \qquad b = 2(2\beta_i^2 - \omega_i^2), \qquad c = \omega_i^4.$$

Equation (4.2) represents a parabola, whose minimum occurs at

$$x_{\min} = -\frac{b}{2a} = \omega_i^2(1 - 2\beta^2/\omega_i^2). \tag{4.3}$$

From eq. (4.3), considering that $\beta_i/\omega_i \simeq 1/(2Q) \simeq 10^{-6} \ll 1$, we derive

$$\omega_i \simeq \sqrt{x_{\min}}. \tag{4.4}$$

In practice we evaluate the resonance frequency ω_i using the parameters a and b obtained from a fit of the spectral data to a parabola.

The decay times may be estimated from the bandwidth of the resonance peaks

$$\tau_i = 1/\beta_i = \frac{2}{\Delta\omega_i}, \tag{4.5}$$

where $\Delta\omega_i$ is the width of the spectral peak.

But the spectra we estimate are different from the actual spectra. More precisely, if $L(\omega)$ is the power spectrum, its estimate $L^{\text{est}}(\omega)$ is the convolution $L(\omega) * W(\omega)$, where $W(\omega) = \sin^2(\omega T)/(T\pi\omega)^2$ is the Fourier transform of the time window of duration T used for the data [11, 12]. The frequency dependence of the estimated spectra is therefore different from the Lorentzian behaviour, depending also on the time T.

Figure 12 shows the Lorentzian curve, the window and the convolution of the two, for $T = 10$ minutes and for $T = 2$ hours, in both cases using $\tau_i = 2000$ s: the width of the spectral estimate considerably differs from the expected Lorentzian behaviour when T is 10 minutes, that is $T < \tau_i$.

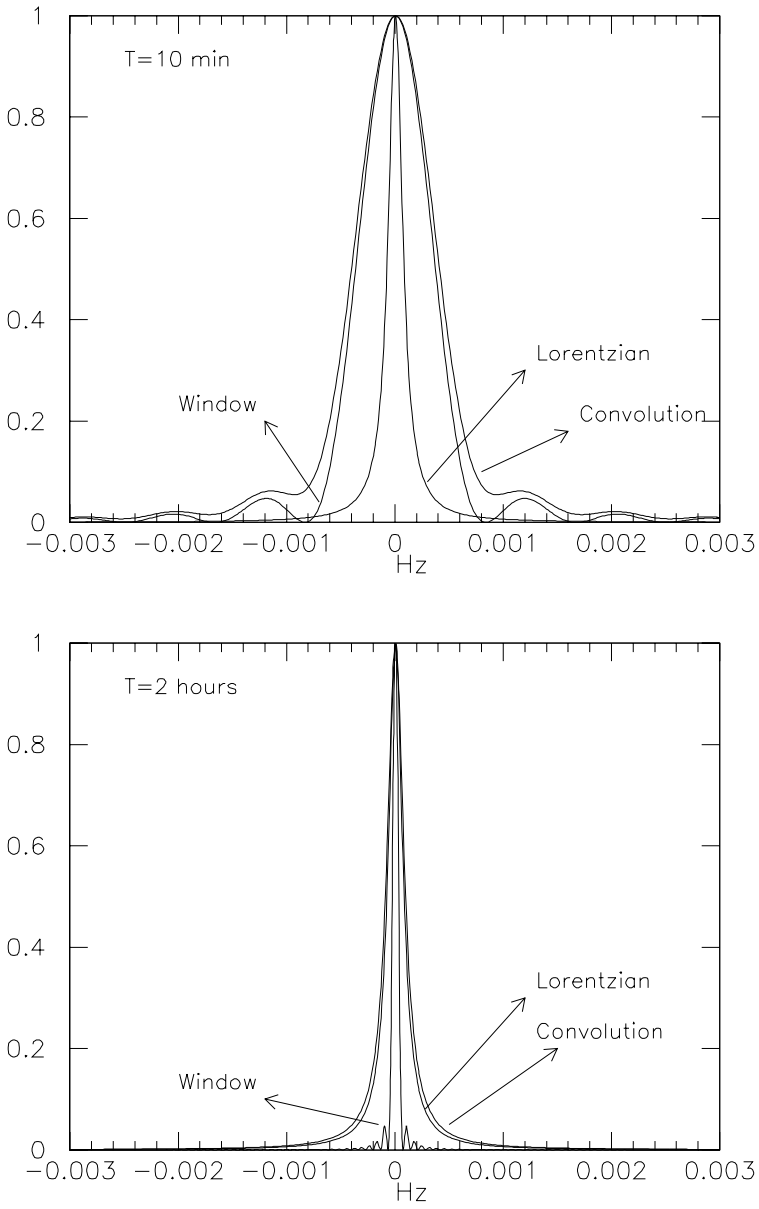

Fig. 12. – Lorentzian curve, window and convolution of the two, for $T = 10$ minutes and $T = 2$ hours. The Lorentzian curves are constructed with $\tau = Q/(2\omega_0) = 2000$ s. It is possible to note that the spectral estimation considerably differs from the Lorentzian behaviour when T is 10 minutes.

As a consequence, to construct the matched filter, we use the values of the coefficients β_- and β_+ obtained from direct measurements on the apparatus, instead of estimating them from the spectra.

The frequency estimation algorithm, on the other hand, provides good results also using windowed data, with errors of $\simeq 0.01$ mHz ([5]) using $T = 10$ min.

As regards the estimation of the resonance frequencies, tests performed on simulated data obtained using the 1991 and 1994 parameters of the Explorer detector gave the following results:

Frequencies for Explorer 1991

actual values	$\nu_- = 904.80167$	$\nu_+ = 921.38023$	Hz
estimates	$\nu_- = 904.80160$ $(\sigma = 4 \cdot 10^{-5})$	$\nu_+ = 921.38040$ $(\sigma = 1 \cdot 10^{-5})$	Hz

Frequencies for Explorer 1994

actual values	$\nu_- = 907.05129$	$\nu_+ = 923.26330$	Hz
estimates	$\nu_- = 907.05123$ $(\sigma = 1 \cdot 10^{-5})$	$\nu_+ = 923.263300$ $(\sigma = 4 \cdot 10^{-6})$	Hz

In the above estimations we note the presence of a systematic error, always less than 0.2 mHz. We found that this error is due to the position of the resonance frequencies with respect to the discrete frequencies of the spectrum. Its consequences on the overall performance of the filter are discussed in subsect. **4**˙2.

The estimation of the coefficients β_- and β_+ becomes more satisfactory when we consider the data processed by means of lock-in amplifiers. In this case, performing an estimation on a time $T \simeq 2$ hours requires an FFT on 32768 samples (corresponding to 2.63 hours). We have applied the algorithm to the spectrum of one mode (ν_+), obtained by averaging 14 periodograms each done on 32768 samples (for a total time of 36 hours). We have obtained $\tau = 2721$ s with a standard deviation of 367 s on a file of April 1994 where the measured τ value was 2066 s. We have also applied the estimation to a file of February 1994 where the measured τ value was higher, 4000 s. We have obtained $\tau = 3376$ s with a standard deviation of 323 s. We remark that this procedure, that requires long periods of data to perform the estimation, has to face the problems of the non-stationarity in the data.

4˙3. *Adaptive matched-filter transfer function.* – The performance of the matched filter may be degraded by the imperfect knowledge of the parameters required for building the filter, the effect of time variations of these parameters and also by a possible inadequacy of the model used to represent the noise (assumed as the superposition of two Lorentzian curves and a flat spectrum). To overcome these problems we use adaptive filters, whose parameters are derived from the estimation of the actual noise spectrum of the data and are therefore periodically updated. Typically, we update the filter every two hours, when we perform a new spectral estimation.

In order to construct the matched-filter transfer function, given by eq. (3.3), it is necessary to evaluate the Fourier transform of the signal $u(t)$, eq. (1.21), that is the transducer displacement when the input force acting on the bar is a delta-function.

([5]) The resonance frequencies of the apparatus are measured in hardware with an error of ± 0.2 mHz.

Since we are now dealing with sampled and aliased data, we consider

$$u(n\,\Delta t_f) = U_1 \exp\left[-\frac{n\,\Delta t_f}{\tau_1}\right] \sin(\omega'_-\, n\,\Delta t_f) + U_2 \exp\left[-\frac{n\,\Delta t_f}{\tau_2}\right] \sin(\omega'_+\, n\,\Delta t_f), \tag{4.6}$$

where $\Delta t_f = 18.18$ ms is the sampling time, n an integer index, $\omega'_- = \omega_- - (900.02677 \cdot 2\pi)$ and $\omega'_+ = \omega_+ - (900.02677 \cdot 2\pi)$ are the aliased angular resonance frequencies, and $V_1 = \omega_-/(m_x(\omega_+^2 - \omega_-^2)) \simeq -V_2 = -\omega_+/(m_x(\omega_+^2 - \omega_-^2))$ are the amplitudes.

Figure 13 shows $u(n\,\Delta t_f)$, computed using the parameters of Explorer 1991, over two different time scales.

The filter transfer function is

$$H(jn\,\delta\nu_l) = \frac{U^*(jn\,\delta\nu_l)}{S_t(n\,\delta\nu_l)}, \tag{4.7}$$

where $U(jn\,\delta\nu_l)$ is the discrete Fourier transform of $u(n\,\Delta t_f)$ and $S_t(n\,\delta\nu_l)$ is the power spectrum, estimated by averaging spectra obtained from 4096 samples (corresponding to the frequency range 900.026, 955.026 Hz with resolution $\delta\nu_l = 13.36$ mHz).

Figure 14*a*) shows the matched filter transfer function obtained with the above procedure for the two hours of the 1991 data, whose spectrum is shown in fig. 11*a*).

Figure 14*b*) shows the same function for the two hours of the 1994 data, whose spectrum is shown in fig. 11*b*).

The spectral gain, defined by eq. (3.5) is computed with the expression

$$G(n\,\delta\nu_l) = \frac{|U(jn\,\delta\nu_l)|^2}{S_t(n\,\delta\nu_l)} \tag{4.8}$$

and the filter gain R_0, defined by eq. (3.23), is computed with the expression

$$R_0 = \delta\nu_l \cdot 2\left(\sum_{n=1}^{2048} G(n\,\delta\nu_l)\right). \tag{4.9}$$

Figures 15*a*) and *b*) show the spectral gain for the data of fig. 11*a*) (1991) and 11*b*) (1994). Note that the 1994 spectral gain is significantly different from zero only in a very narrow band around both the resonances, less than 2 Hz, while in 1991 the bandwidth is of the order of $\simeq 4$ Hz for both the modes.

In order to express the filtered data in terms of energy innovation in the bar in units of kelvins, we multiply the filter transfer function with the volt-to-$\sqrt{\text{K}}$ conversion factor Y. This quantity is obtained by putting $T_s = 1$ K in eq. (1.41), which expresses the voltage signal at the output of the instrumentation when the bar is excited by an energy burst of $E_s = kT_s$ joules. We obtain

$$\sqrt{Y} = \frac{1}{\alpha AB}\sqrt{\frac{m_x}{2k}}\left[\frac{(\omega_+^2 - \omega_-^2)}{(\omega_+ + \omega_-)}\right]\left(\frac{\sqrt{\text{K}}}{\text{V}}\right), \tag{4.10}$$

with A and B given by eqs. (1.39) and (1.40).

The quantity A is evaluated in frequency domain from the data spectrum with lower frequency resolution. Hence its value is updated every two hours.

Figure 16 shows *a*) the system response (in volts) to a simulated input burst

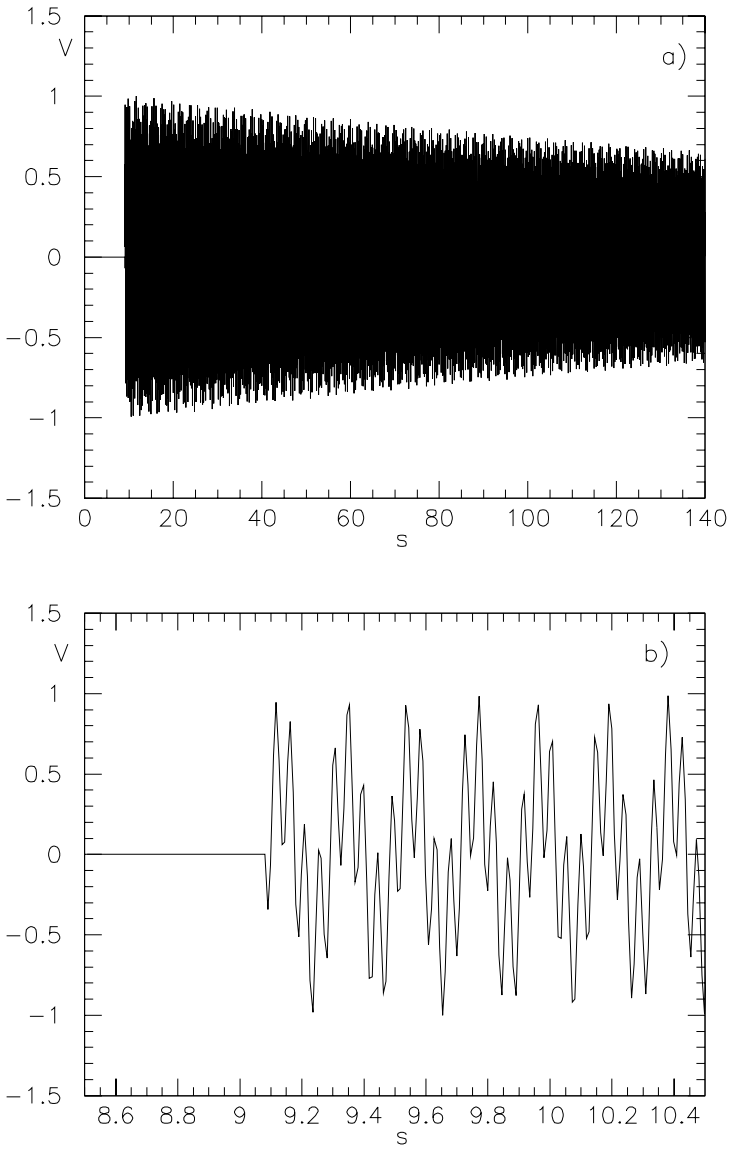

Fig. 13. – Impulse response at the transducer computed with the parameters of Explorer 1991. The signal arrives at the time $t = 9.07$ s. In *a*) it is possible to note the exponential decay and in *b*) the beating due to the two resonances.

of known energy $T_s = 5.98$ K; *b*) the filtered signal in kelvins whose maximum is 5.98 K, as expected.

Then, the filter transfer function, including the normalization, is

$$H'(jn\,\delta\nu_l) = \frac{U^*(jn\,\delta\nu_l)\sqrt{Y}}{S_t(n\,\delta\nu_l)\,R_0}\,. \tag{4.11}$$

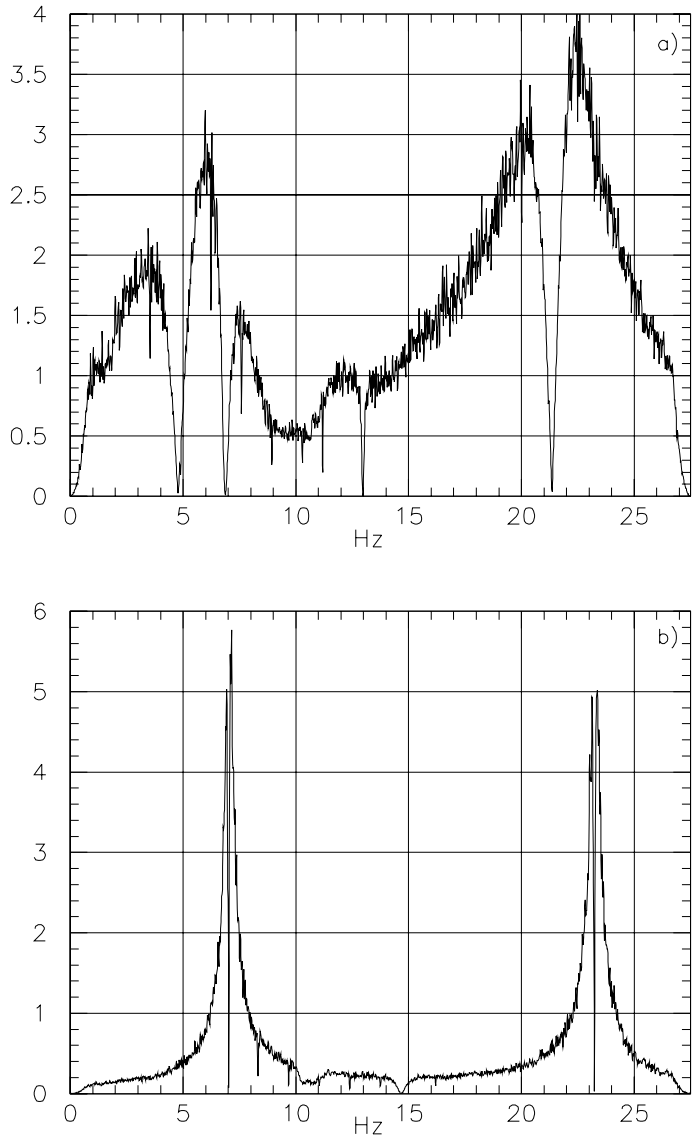

Fig. 14. – Matched filter transfer function for the two hours, whose spectra are shown in fig. 11*a*) (1991) and 11*b*) (1994).

The discrete signal $g(n\,\Delta t_f)$ at the matched filter output, if the input force acting on the bar is a delta-function, in the absence of noise, is (see eq. (3.14))

$$g(n\,\Delta t_f) = V_1 \exp\left[-\beta_{3+}\,|n\,\Delta t_f|\right] \cos\left(n\omega_+\,\Delta t_f\right) + \tag{4.12}$$

$$+ V_2 \exp\left[-\beta_{3-}\,|n\,\Delta t_f|\right] \cos\left(n\omega_-\,\Delta t_f\right),$$

with $V_1 \simeq V_2$ and $\beta_{3\pm} = \beta_{1\pm}/\sqrt{\Gamma_\pm}$.

Figure 17 shows $|g(n\,\Delta t_f)|^2$, expressed in kelvins, for the Explorer 1991 and 1994.

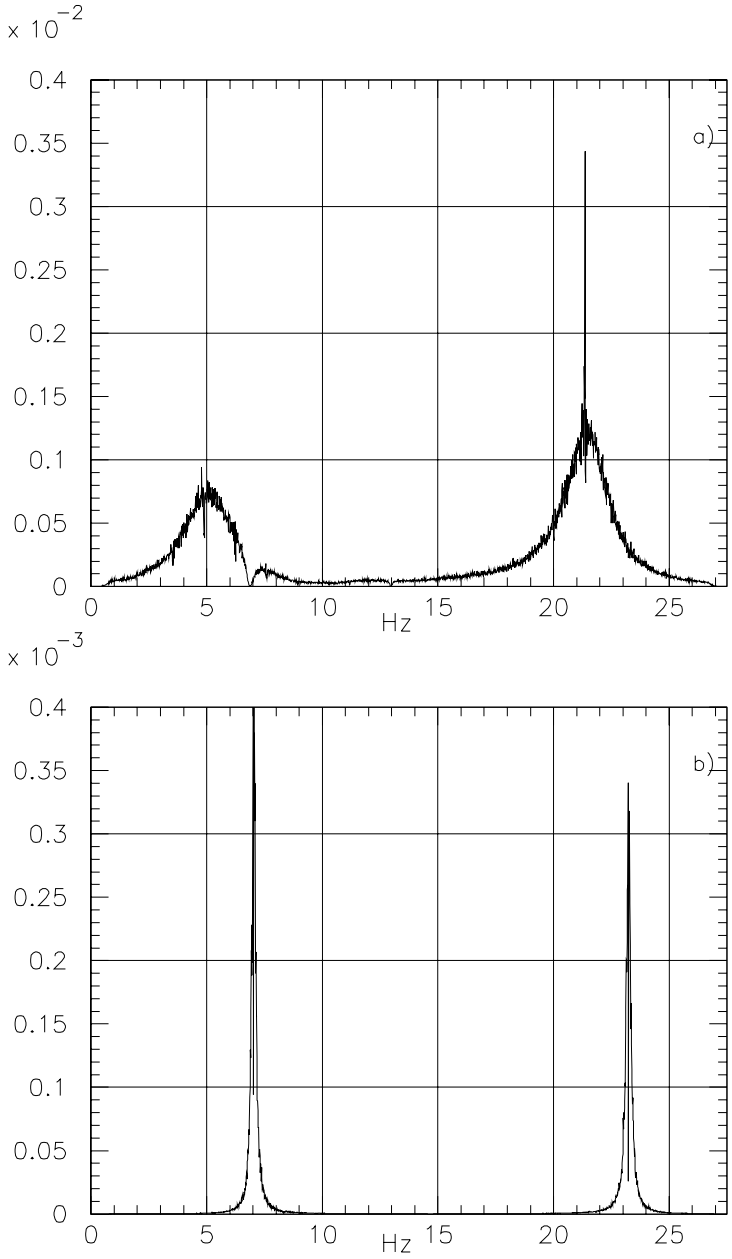

Fig. 15. – Spectral gain for the two hours, whose spectra are shown in fig. 11*a*) (1991) and 11*b*) (1994).

4˙4. *Discretization effects.* – We have shown in sect. **3**˙2 that the effective temperature T_{eff}, that represents the minimum detectable energy, is the same for both the "fast" and the "slow" data filtering procedures. But this is a theoretical result, derived considering continuous time ideal filters.

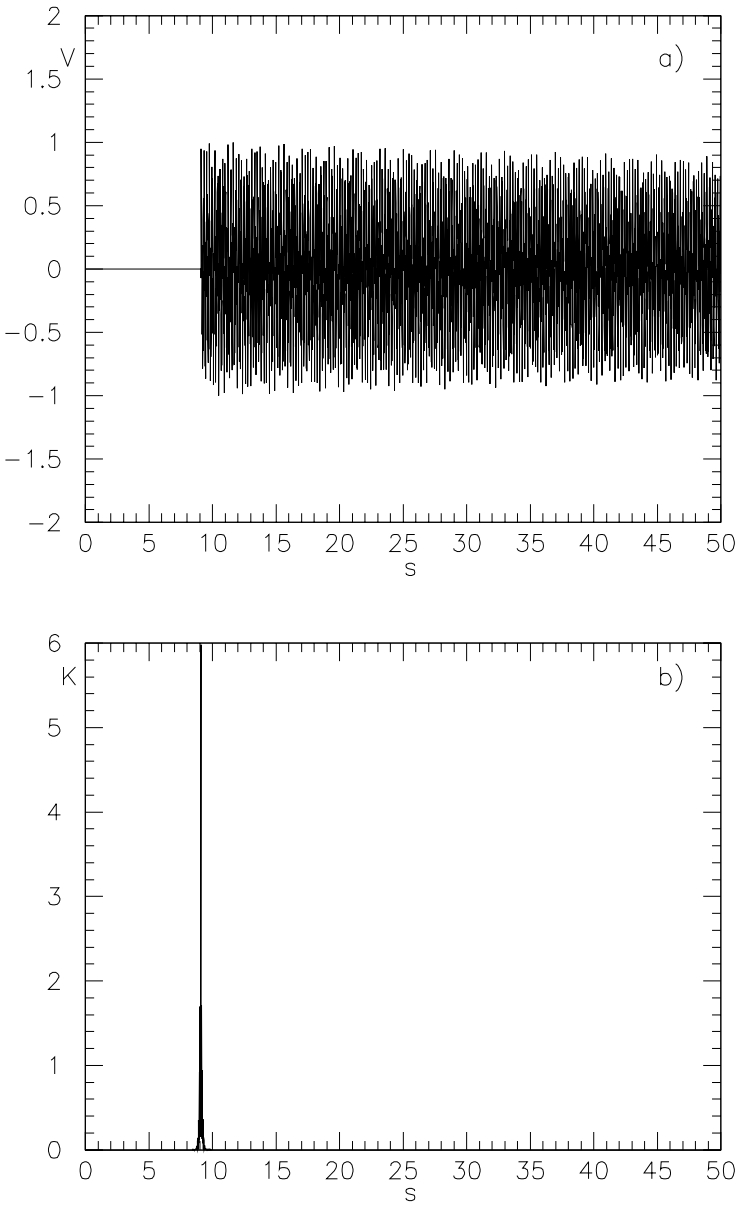

Fig. 16. – *a*) Transducer output, volts *vs.* time (s), *b*) matched filter output $|g(t)|^2$, kelvins *vs.* time (s), when an input delta signal is applied to the bar at $t = 9.07$ s, with the parameters of the Explorer detector during 1991.

The results obtained in practice, dealing with sampled data processed by discrete time filters, may be somewhat different, depending both on the values of the sampling time and of the parameters of the experimental apparatus, due to various discretization effects that degrade the filtering performance.

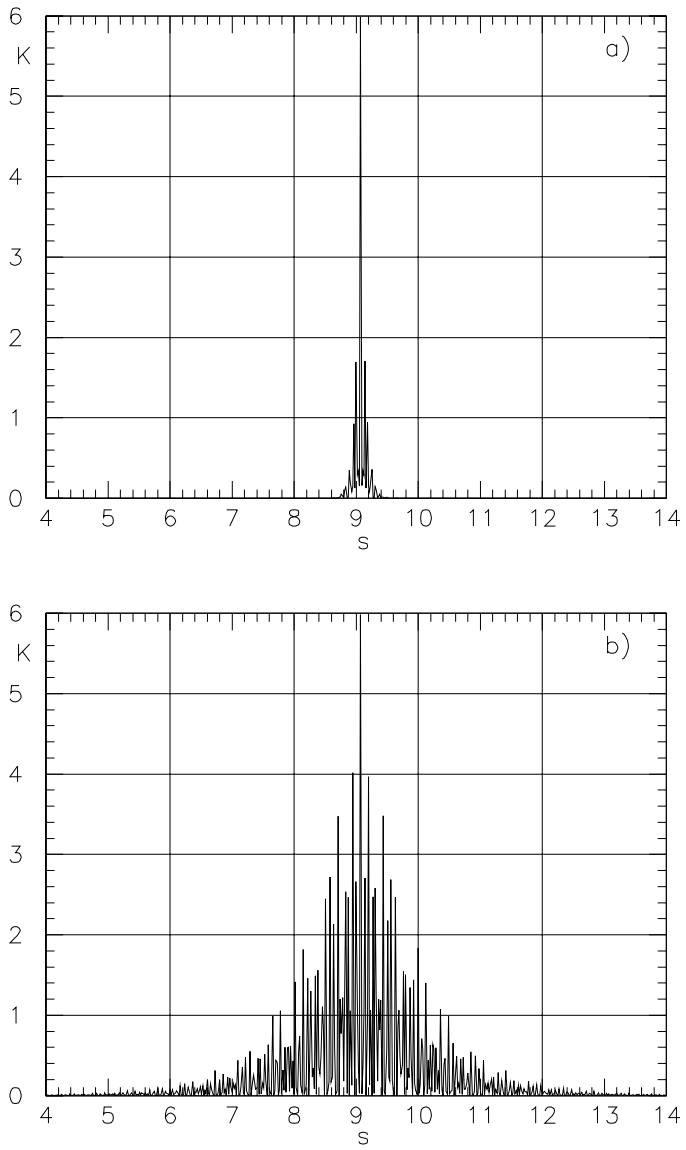

Fig. 17. – Matched filter response $|g(t)|^2$ to an input delta signal of energy $E_s = k \cdot 598$ joules, for the Explorer detector with the 1991 (*a*)) and 1994 (*b*)) parameters (see table II).

An analysis of these effects for the "slow" filtering procedure has been reported in [6]. We discuss in what follows the case of the "fast" filtering procedure.

4˙4.1. Dependence on the "phase" of the input signal. When dealing with discrete time data, the maximum amplitude of the impulse response depends on the arrival time of the input delta-function with respect to the sampling time interval, which we call the "phase" Ψ of the input signal.

When the phase is zero, that is the input delta function is synchronized with the

sampling time, the above maximum coincides with the theoretical value. It decreases for increasing values of the phase, with the minimum value typically obtained when the signal arrival time occurs near one half of the sampling period ($\Psi \simeq 0.5$). This effect reduces the SNR and therefore increases the actual effective temperature of the detector. For the "slow" filtering procedure [6], we have found that it strongly depends on the product $\beta_3 \Delta t$.

In the tables below we report the results obtained for both the "fast" ($\Delta t_{ff} = 4.544$ ms) and the "slow" (at the two modes) filtering procedures using simulated data with the parameters of Explorer 1991 and 1994, that is with $\beta_{3-} \Delta t_s = 1.43$ and $\beta_{3+} \Delta t_s = 0.90$ for the 1991 data; $\beta_{3-} \Delta t_s = 0.13$ and $\beta_{3+} \Delta t_s = 0.12$ for the 1994 data. Those results have been obtained by averaging the data corresponding to ten different values of the arrival phase Ψ, from 0 to 0.9, thereby simulating random arrival times.

Explorer 1991

	Fast filter	Slow filter
Reduction of the square of the max amplitude	$r = 0.92$	$r_- = 0.68$, $r_+ = 0.74$
Relative standard deviation	$\sigma = 0.06$	$\sigma_- = 0.28$, $\sigma_+ = 0.21$

Explorer 1994

	Fast filter	Slow filter
Reduction of the square of the max amplitude	$r = 0.98$	$r_- = 0.95$, $r_+ = 0.95$
Relative standard deviation	$\sigma = 0.01$	$\sigma_- = 0.03$, $\sigma_+ = 0.03$

The above results show that this effect is rather weak for the 1994 data, while it degrades the "slow" data sensitivity by a factor $\simeq 1.5$ in the 1991 data where the product $\beta_3 \Delta t$ is ten times larger than in the 1994 data. This is consistent with the results of the analysis on the real Explorer data, reported in sect. **5**.

We now want to show the results we obtain when considering the sampling time of $\Delta t_f = 18.18$ ms. As shown in the table below, the effect for the fast filter with $\Delta t_f = 18.18$ ms is stronger, as expected because of the greater sampling time.

Explorer, data sampled with $\Delta t_f = 18.18$ ms

	1991	1994
Reduction of the square of the max amplitude	$r = 0.743$	$r = 0.904$
Relative standard deviation	$\sigma = 0.269$	$\sigma = 0.06$

For data sampled at $\Delta t_f = 18.18$ ms, fig. 18 shows the filtered response for different phases, fig. 19 shows the reduction of the square of the maximum amplitude of the filtered signal as a function of the phase of arrival (normalized to the maximum obtained at $\Psi = 0$). The smallest amplitude of the maximum occurs for $\Psi = 0.5$, when two consecutive samples take about the same value. An interesting parameter is the

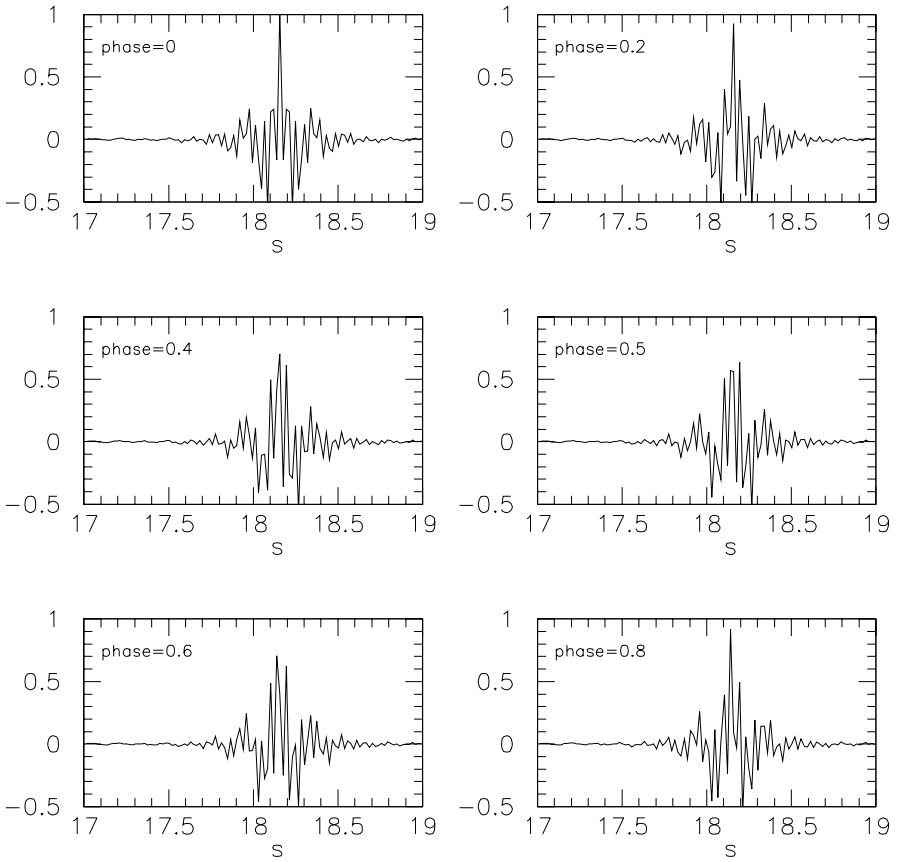

Fig. 18. – Dependence on the "phase" Ψ of the input delta signal: matched filter response $g(t)$. The parameters are those of Explorer 1991, with a sampling time of 18.18 ms. The response is distorted when the phase is different from zero; the maximum reaches its minimum value for $\Psi = 0.5$.

ratio of the amplitude of the main peak of the signal to the amplitude of the sidelobes. According to eq. (4.12), the two first side lobes occur with respect to the main lobe at times $1/\nu_+ \simeq \pm 48$ ms, and $1/\nu_- \simeq \pm 142$ ms. The above ratio is maximum for $\Psi = 0$ and decreases as Ψ moves to 0.5, when it reaches its minimum value.

For the impulse responses computed with the parameters of Explorer 1991, this ratio is larger than unity for any value of Ψ. While using the parameters of Explorer 1994 the ratio decreases below 1 (for $\Psi = 0.5$): this means that the maximum of the response, in this case, is displaced from the time of application of the burst (the error is ± 142 ms). Figure 20 shows this situation: we have plotted the filter response for $\Psi = 0$ and $\Psi = 0.5$ on two different time scales in order to have both the whole behaviour of the response and its behaviour near the time t_i. We note, moreover, that the presence of noise may alter the waveform, introducing an additional cause of uncertainty for the timing of an event.

As a conclusion, the reduction of SNR due to different phases of arrival of the input signal is a function of $\beta_3 \Delta t$, as for the "slow" data, and the amplitude reduction is

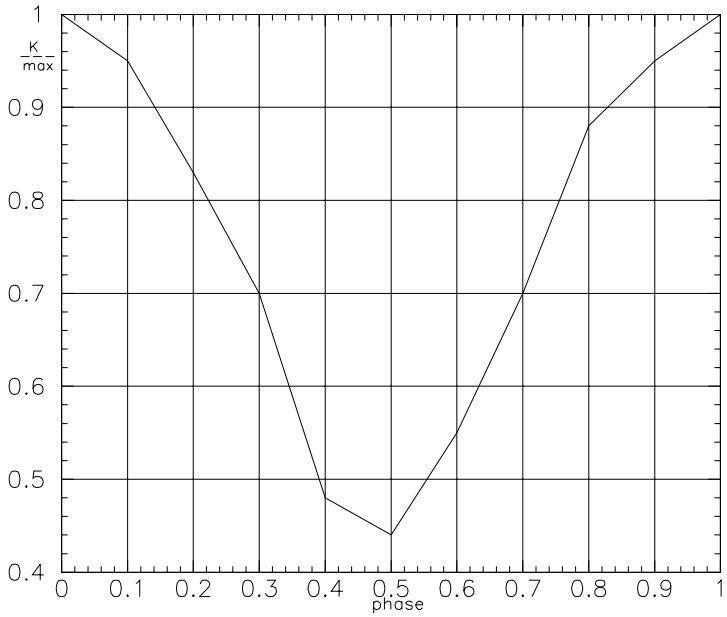

Fig. 19. – Dependence on the "phase" Ψ of the input delta signal: reduction of the squared maximum amplitude of the filtered signal $g(t)$ as a function of the phase of arrival of the delta signal.

maximum when the phase is 0.5. The filtered signal is distorted, compared to that obtained with phase equal to zero, and this distortion may affect the determination of the signal arrival time, still depending on the $\beta_3 \Delta t$ value.

4·4.2. Dependence on the resonance frequency. We report here on the dependence of the matched-filter performance on the position of the resonance frequencies with respect to the discrete lines of the spectra used to represent the data, with frequency resolution $\delta\nu_l = 13.36$ mHz (4096 samples with $\Delta t_f = 18.27$ ms).

We have studied this effect by filtering 15 hours of simulated data with fixed values of all the parameters (Explorer 1994) but with different values of the resonance frequencies within the spectral bin width of 13.36 mHz, that is with values $\nu_- = \nu_{0_-} + \alpha\,\delta\nu_l$; $\nu_+ = \nu_{0_+} + \alpha\,\delta\nu_l$.

The frequencies $\nu_{0_-} = 907.05172$ Hz, $\nu_{0_+} = 923.26419$ Hz correspond to exact values of the spectral lines and we have used $\alpha = 0$, 0.25, 0.5 and 0.75.

Figure 21 shows the two power spectra estimated from the simulated data, when the resonance frequencies are equal to the discrete frequencies ($\alpha = 0$) and when they are at $1/2$ of the bin width ($\alpha = 0.5$) near the two resonances. Both the amplitudes and the widths of the peaks are very different in the two cases, as a consequence of the different discretization of the same continuous process. Figure 22 show the spectral gains, around the resonances, for $\alpha = 0$ and $\alpha = 0.5$.

While, ideally, the performance should be the same, we have obtained the following

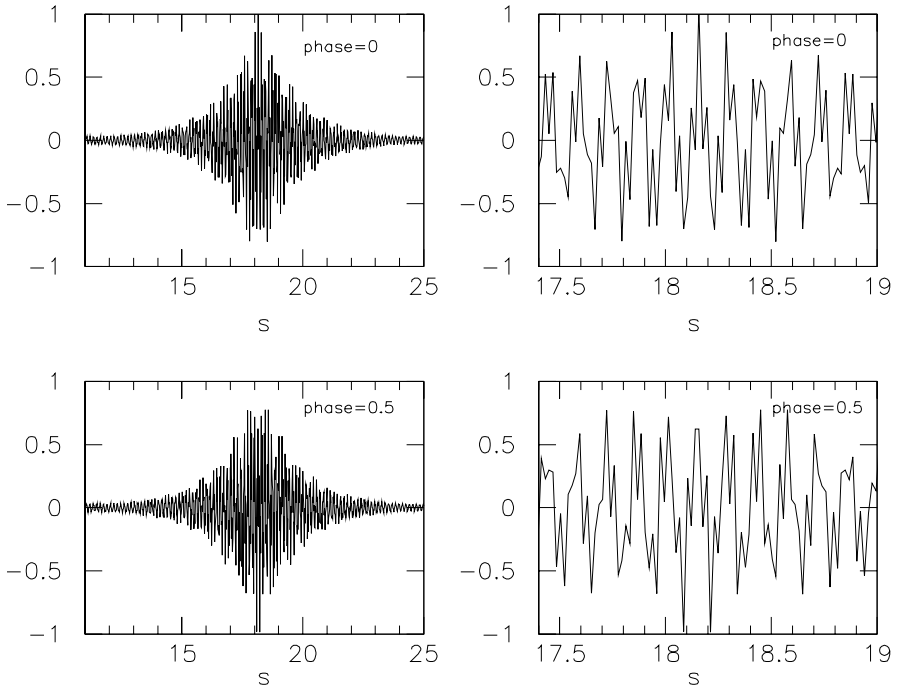

Fig. 20. – Dependence on the "phase" Ψ of the input delta signal: matched filter response $g(t)$ for two different phases of arrival, $\Psi = 0,\ 0.5$. The parameters are those of Explorer 1994, with sampling time of 18.18 ms. The delta signal is applied at the time $t = 18.176$ s.

values of the effective temperatures, and of their dispersion, over 15 hours of simulation:

$$\alpha = 0\,, \qquad T_{\text{eff}} = 8.61\ \text{mK}\,, \quad \sigma = 0.15\ \text{mK}\,,$$

$$\alpha = 0.25\,, \qquad T_{\text{eff}} = 15.12\ \text{mK}\,, \quad \sigma = 0.24\ mK\,,$$

$$\alpha = 0.50\,, \qquad T_{\text{eff}} = 12.30\ \text{mK}\,, \quad \sigma = 0.53\ \text{mK}\,,$$

$$\alpha = 0.75\,, \qquad T_{\text{eff}} = 14.72\ \text{mK}\,, \quad \sigma = 0.33\ \text{mK}\,.$$

Thus, this discretization effect produces, with the parameters of our simulation, a SNR degradation that is, in the worst case, $\simeq 1.7$.

4·5. *Effect of non-optimal choice of the filter parameters.* – In this section we consider the effects due to errors in the parameters used to construct the matched filter. Since the filter is adaptive (the noise spectrum is estimated periodically), the only parameters we need to know are the two resonance frequencies and the two decay times, which determine the function $W_{ux}(j\omega)$, that is the waveform of the expected signal to be filtered (as given by eq. (4.6)). The frequencies are estimated as explained before and the decay times are usually measured experimentally.

When the values of the parameters used for constructing the filter differ from their actual values, the filter is no more adapted to the signal, as shown in the block diagram

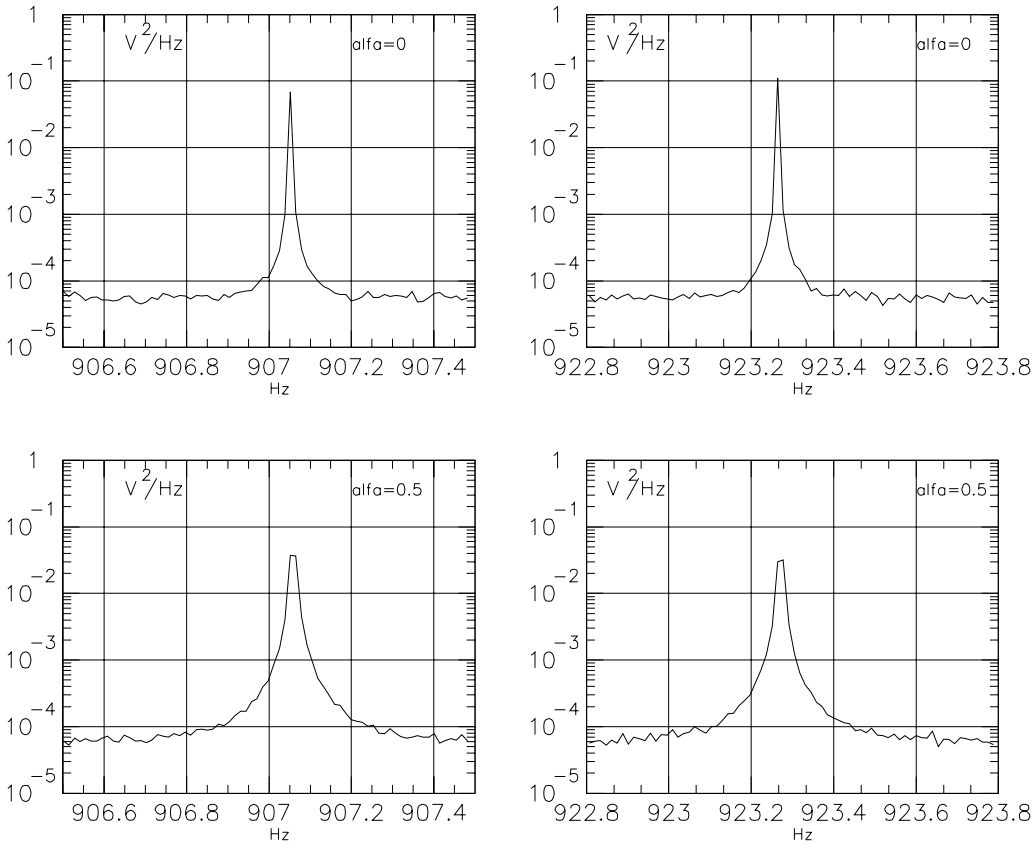

Fig. 21. – Dependence on the position of the resonance frequency. Power spectra around the two resonances, when the resonance frequencies are equal to the discrete frequencies ($\alpha = 0$) and when they are at $1/2$ of the bin ($\alpha = 0.5$). The frequency resolution is $\delta\nu_l = 13.36$ mHz.

of fig. 23, where $W'_{ux} \neq W_{ux}$. In this condition the signal at the filter output is

$$g'(t) = (1/2\pi) \int_{-\infty}^{+\infty} \exp[j\omega t] \frac{1}{S_t(\omega)} \cdot W_{ux}(j\omega)\, W'^{*}_{ux}(j\omega)\, \mathrm{d}\omega \tag{4.13}$$

and the noise variance is

$$\sigma'^2_m = 1/(2\pi) \int_{-\infty}^{+\infty} \frac{1}{S_t(\omega)} \cdot W'_{ux}(j\omega) W'^{*}_{ux}(j\omega)\, \mathrm{d}\omega\,. \tag{4.14}$$

The filter gain is now different for the signal at the noise and the SNR is smaller than its optimal value given by eq. (3.24)

$$(\mathrm{SNR}) = g(0)'^2/\sigma'^2_m. \tag{4.15}$$

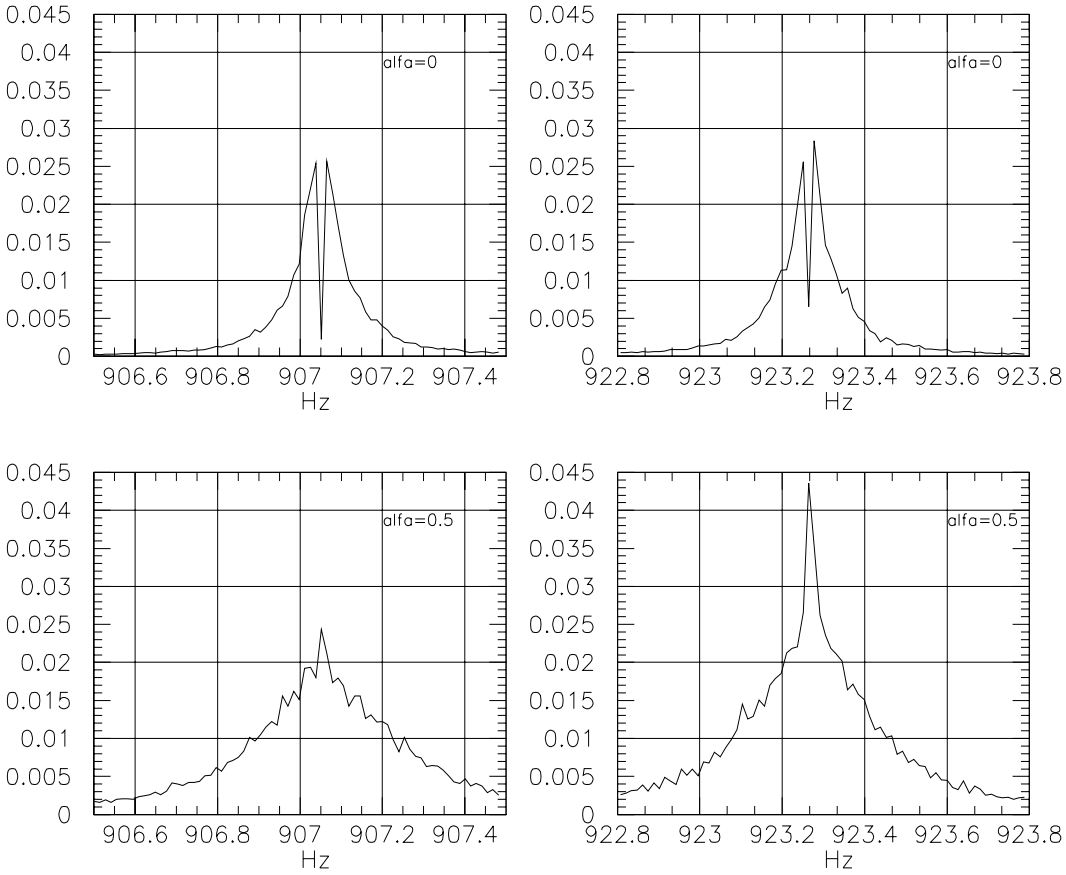

Fig. 22. – Dependence on the position of the resonance frequency: spectral gains around the two resonances, when the resonance frequencies are equal to the discrete frequencies ($\alpha = 0$) and when they are at $1/2$ bin ($\alpha = 0.5$).

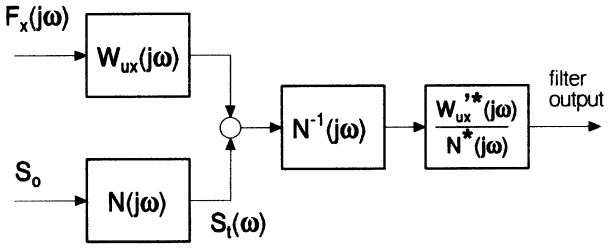

Fig. 23. – Block diagram of the antenna and matched-filter chain, for the case of errors in the parameters of the filter.

4˙5.1. Errors in the resonance frequencies. We consider here the loss of the filter performance due to errors in the resonance frequencies. We have studied this problem by performing simulations, with fixed values of the parameters of the

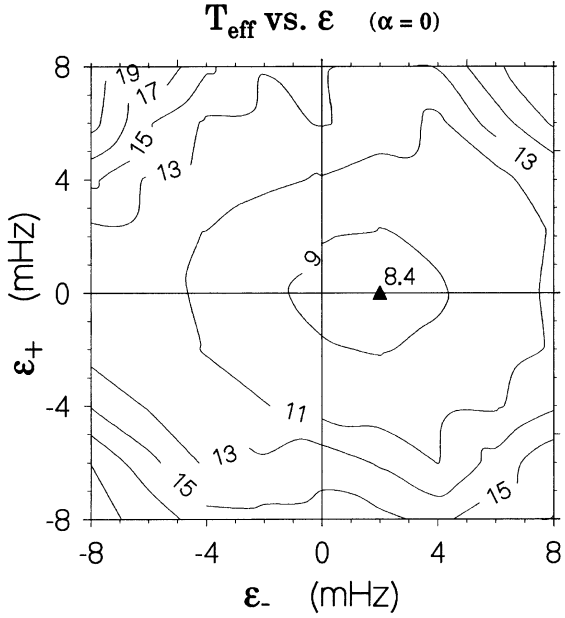

Fig. 24. – Loss of the filter performance due to errors in the resonance frequencies. Dependence of the effective temperature (expressed in mK) on the frequency errors ε_- and ε_+ for $\alpha = 0$.

apparatus (Explorer 1994) but with different values of the resonance frequencies ν_- and ν_+ for the experimental apparatus ($W_{ux}(j\omega)$) and for the filter ($W'_{ux}(j\omega)$): $\nu'_- = \nu_- \pm \varepsilon_-$; $\nu'_+ = \nu_+ \pm \varepsilon_+$.

On the basis of the results of paragraph **4**·4.2, we have considered both the case of ν_- and ν_+ coinciding with spectral lines ($\alpha = 0$) and a few cases of ν_- and ν_+ values in various positions within the spectral bin ($\alpha \neq 0$).

The contour graph of fig. 24 shows the dependence of the effective temperature on the frequency errors ε_- and ε_+ for $\alpha = 0$. Note that the minimum is slightly displaced ($\simeq 2$ mHz) from the origin, but the effective temperature at the origin is only 2% larger than the minimum. Moreover, for larger deviations, the effective temperature increases rapidly.

The results obtained with $\alpha = 0.5$ and $\alpha = 0.25$ are very different: the effective temperature has no definite minima in the region we have explored, with values comprised between $\simeq 11.5$ and $\simeq 12.5$ mK for $\alpha = 0.5$, and between $\simeq 14.5$ and $\simeq 15.5$ mK for $\alpha = 0.25$.

4·5.2. Errors in the decay times. We report here on the effect of errors on the decay times used to construct the matched filter. The analysis has been done using 15 hours of simulated data, with the parameters of the Explorer detector during 1994 ($\tau_- = 1437$ s; $\tau_+ = 2066$ s) and with the resonance frequencies equal to the discrete frequencies, that is with $\alpha = 0$. We have studied the performance of the filters obtained by changing the decay times of the two modes as follows: $\tau'_- = \tau_-/\varepsilon_-$; $\tau'_+ = \tau_+/\varepsilon_+$.

We have evaluated T_{eff} over each one of the 15 hours; in the following table we report the average T_{eff} and its standard deviation.

$\varepsilon(\tau_-)$	$\varepsilon(\tau_+)$	$T_{\rm eff}$ (mK)	σ (mK)
0.001	0.001	8.67	0.15
0.01	0.01	8.67	0.15
1	1	8.61	0.15
10	10	8.64	0.19
1000	1000	10.64	0.16

The above results show that the effective temperature is quite unaffected by the use of wrong values of the decay times, even for large deviations of these quantities. Thus, we conclude that the time decay values do not represent a critical point for the adaptive filter realization.

4˙5.3. Phase shift between the two resonances. In subsect. **1**˙4 we have considered the impedance of the electrical circuit at the transducer output, given by eq. (1.33), which we have taken constant in the frequency range of our interest. This is not exactly true, and as a result there may be a phase shift of the response between the two resonances, which we evaluated to be smaller than 0.1 rad, in all practical cases. The results of a simulation performed to study the effect of this phase shift on the effective temperature show that it is totally negligible.

5. – Experimental results with the Explorer data

5˙1. *Explorer 1991.* – We report here the results obtained by filtering the data of the Explorer detector from June 19 to December 16, 1991, whose parameters are given in table II, in subsect. **4**˙1, and by comparing the events found with different filtering procedures.

We have excluded from the analysis the data recorded during tests and cryogenic refillings or with clear signs of unproper functioning of the apparatus. In addition, we have used the auxiliary channels as vetoes for eliminating the data collected in the presence of disturbances in the laboratory. The effective number of days is 122 days, corresponding to a duty cycle of 67%. These data have been filtered with both the procedures discussed in this work:

"slow" filtering, *i.e.* adaptive Wiener filter, with selection of the minimum (see sect. **2**), applied to the data processed by lock-in amplifiers and sampled with $\Delta t_{\rm s} = 290$ ms;

"fast" filtering, *i.e.* adaptive matched filter applied to the data sampled with $\Delta t_{ff} = 4.5$ ms.

The theoretical values of the sensitivity, computed using the known parameters of the experimental apparatus, are the same for the two cases: $T_{\rm eff}^{\rm theor} \simeq 4$ mK, which means that the "apparent" temperature of the "fast" filter (over the scale normalized to the peak value of the signal) should be $\simeq 2$ mK. The best experimental values obtained are:

"slow" filter: $T_{\rm eff} \simeq 8\,{\rm mK}$ (corresponding to $h \simeq 7.1 \cdot 10^{-19}$, see [1]),

"fast" filter : $T_{\rm eff} \simeq 4\,{\rm mK}$ (corresponding to $h \simeq 5.1 \cdot 10^{-19}$).

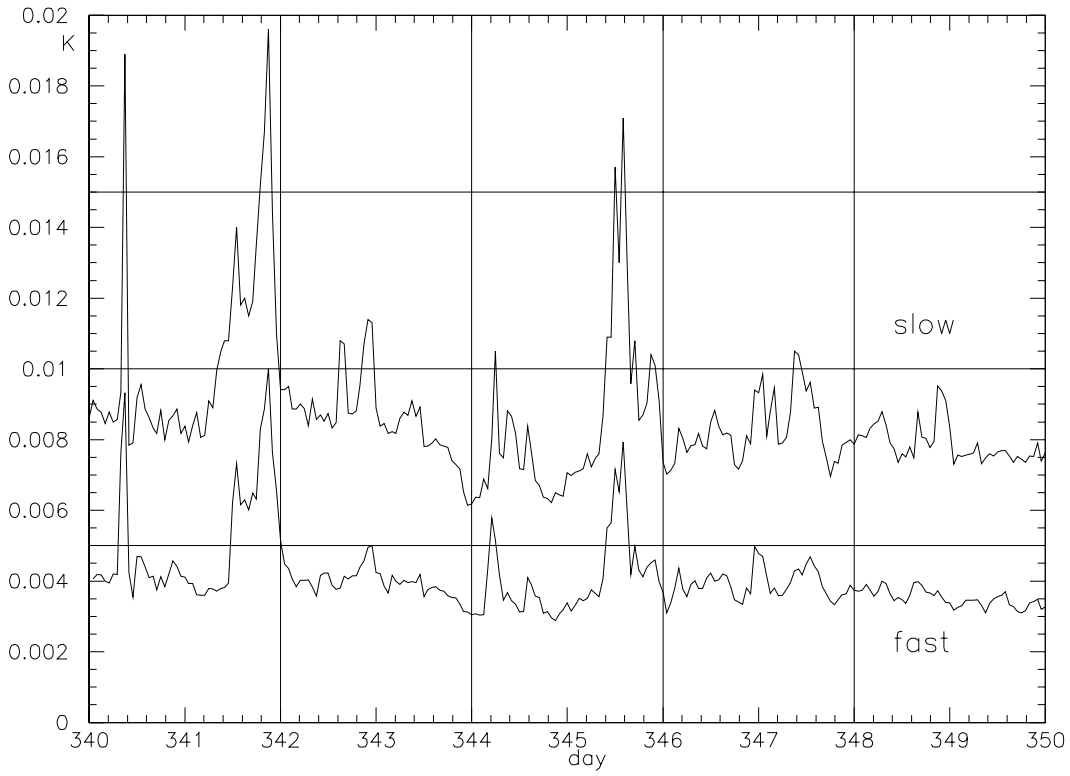

Fig. 25. – Effective temperatures (hourly averages) of the "slow" and "fast" filtered data for 10 days during December 1991.

Figure 25 shows the hourly averages of the effective temperatures, for 10 days during December, of the "slow" and "fast" filtered data, both a factor of 2 above the theoretical value.

We have done a simulation to compare the results obtained from the two different analysis procedures (using the parameters of Explorer 1991). We have added to the noise process a number of standard signals, with very large signal-to-noise ratio and with different phases of arrival with respect to the sampling time. Using 40 events of energy 20 K we have obtained $\mathrm{SNR}_{\mathrm{fast}}/\mathrm{SNR}_{\mathrm{slow}} \simeq 2.5$. This means that the fast procedure has an overall sensitivity for the detection of bursts with random phases of arrival a factor of 2.5 better than the slow procedure, in fair agreement with the result obtained using the real Explorer data as well with the theoretical value of 2.

Considering again the data collected by Explorer, the number of events with energy above the threshold of 80 mK are $N_{\mathrm{slow}} = 25098$ and $N_{\mathrm{fast}} = 19440$. Figure 26 shows the two distributions.

We have searched for coincidences between these two streams of events. Since they originate from the experimental data of the same detector using two optimum filters both aiming at detecting short bursts of g.w. radiation, we expected a very large number of coincidences. But the number of coincident events between the two data streams is only 187, within a window of ± 0.15 s, that is only 1% of the total events. For

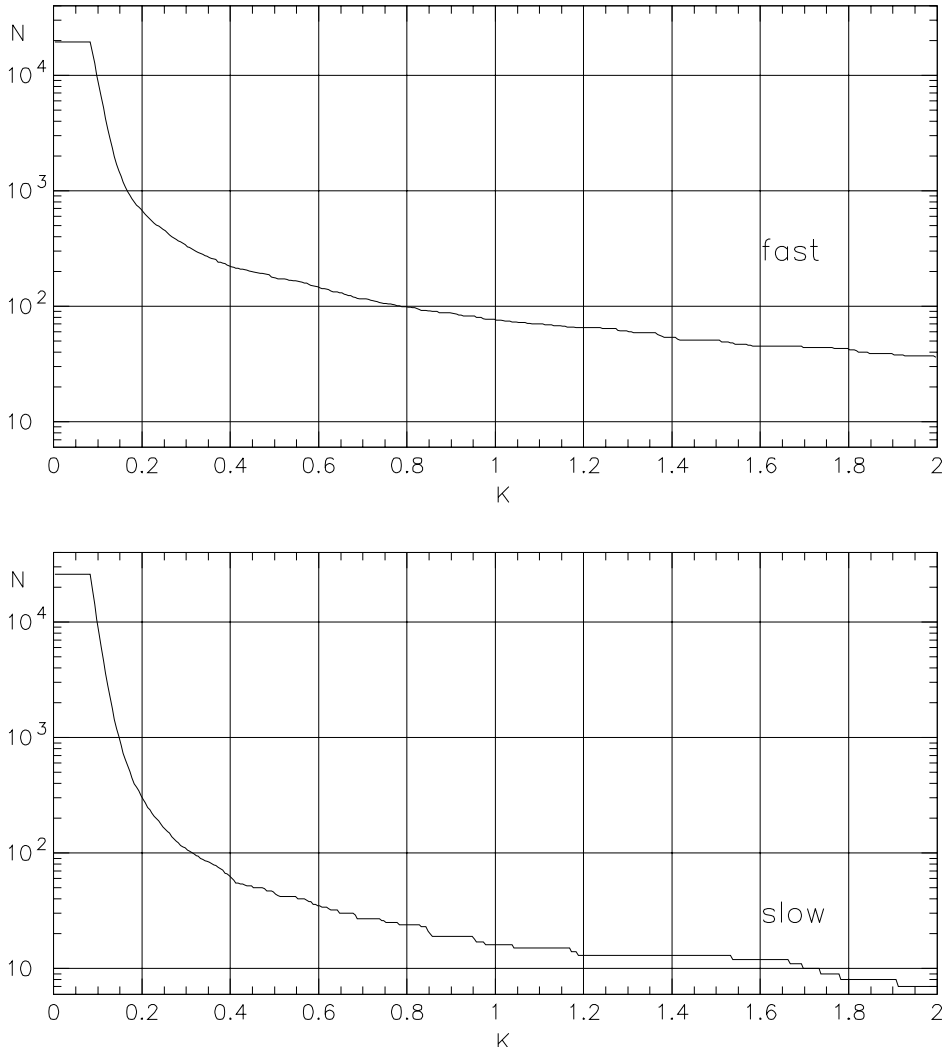

Fig. 26. – Integral distributions of the filtered events for 6 months of data in 1991, obtained with the "fast" and the "slow" filters.

the understanding of the problem we have performed a simulation analysis, that is we have processed with both the "fast" and the "slow" procedures simulated data consisting *a*) of noise only, *b*) of noise plus the response to "short" and "long" excitations (with various values of SNR). The results of this analysis are reported in [13, 14]: we found that the events due to noise fluctuations and those due to "long" excitations were different in the two cases. Only those events due to input delta forces, with very large SNR, were seen at the same time by both the filters.

5˙2. *Explorer 1994.* – As shown in table II, subsect. **4**˙1, the Explorer parameters during the 1994 run were very different from 1991, in particular the overall bandwith being smaller roughly by a factor of ten. In subsect. **4**˙3 we have shown how different

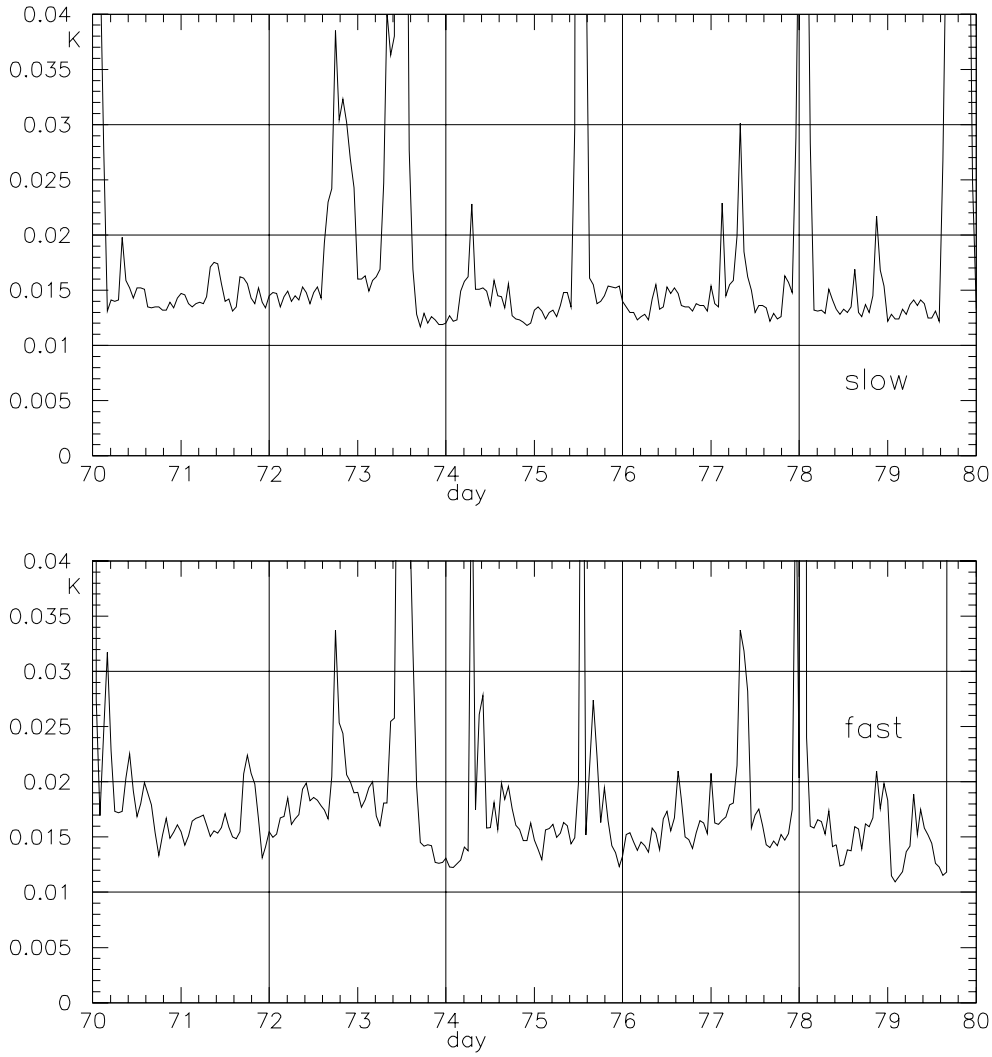

Fig. 27. – Effective temperatures (hourly averages) of the "slow" and "fast" filtered data for 10 days during March 1994.

the two spectral gains are (see fig. 15*a*), *b*)). Hence, with these parameters, we do not expect a big improvement of the "fast" filter with respect to the "slow".

Figure 27 shows the hourly averages of the effective temperature for both the filters (here again considering the "apparent" temperature for the "fast" filter), during ten days in March 1994, from day 70 to day 80. The level is of the order of 14 mK for the "slow" data, and of 15-16 mK for the "fast" data.

Figure 28 shows the same data for 4 days from 29 March to 1 April (days 88 to 92). Here the level is of the order of 10 mK for the "fast" data and still of the order of 14 mK for the "slow" data.

We have investigated the reason for this change of performance of the "fast" filter,

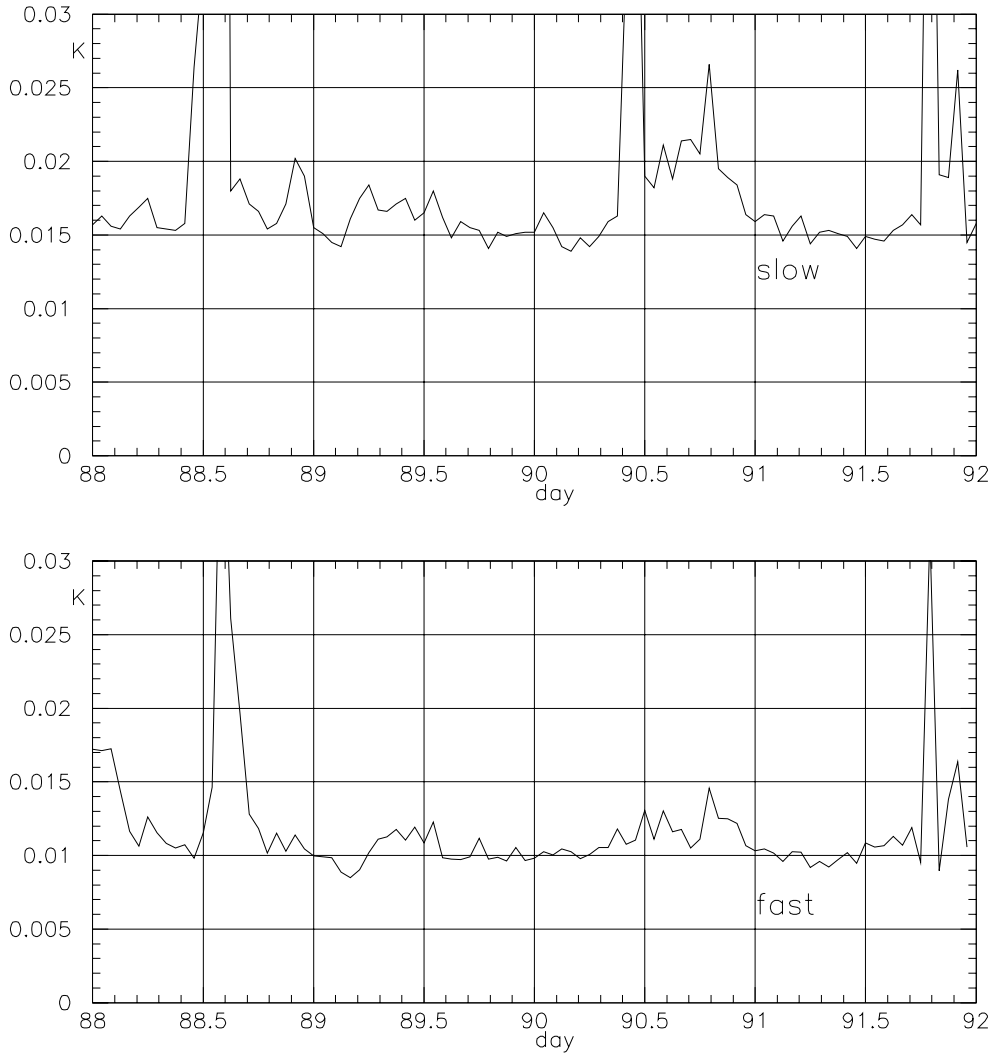

Fig. 28. – Effective temperatures (hourly averages) of the “slow” and “fast” filtered data for 4 days in March-April 1994.

occurring after few days with no evident modifications of the experimental apparatus. We found that the above effect is related to a small variation of the resonance frequencies of the detector, as shown in fig. 29 from day 80 to day 82 the frequency ν_- changes abruptly from 907.0475 Hz to 907.051 Hz, and ν_+ from 923.261 Hz to 923.2633 Hz. This is due to the fact that on day 80 the working point of the SQUID was changed (it can be shown experimentally that a working point change may cause a variation in the resonance frequency of a few mHz).

Note that the latest frequencies almost coincide with discrete frequencies of the spectrum (907.05172 Hz and 923.26419 Hz). For this reason, the loss of performance

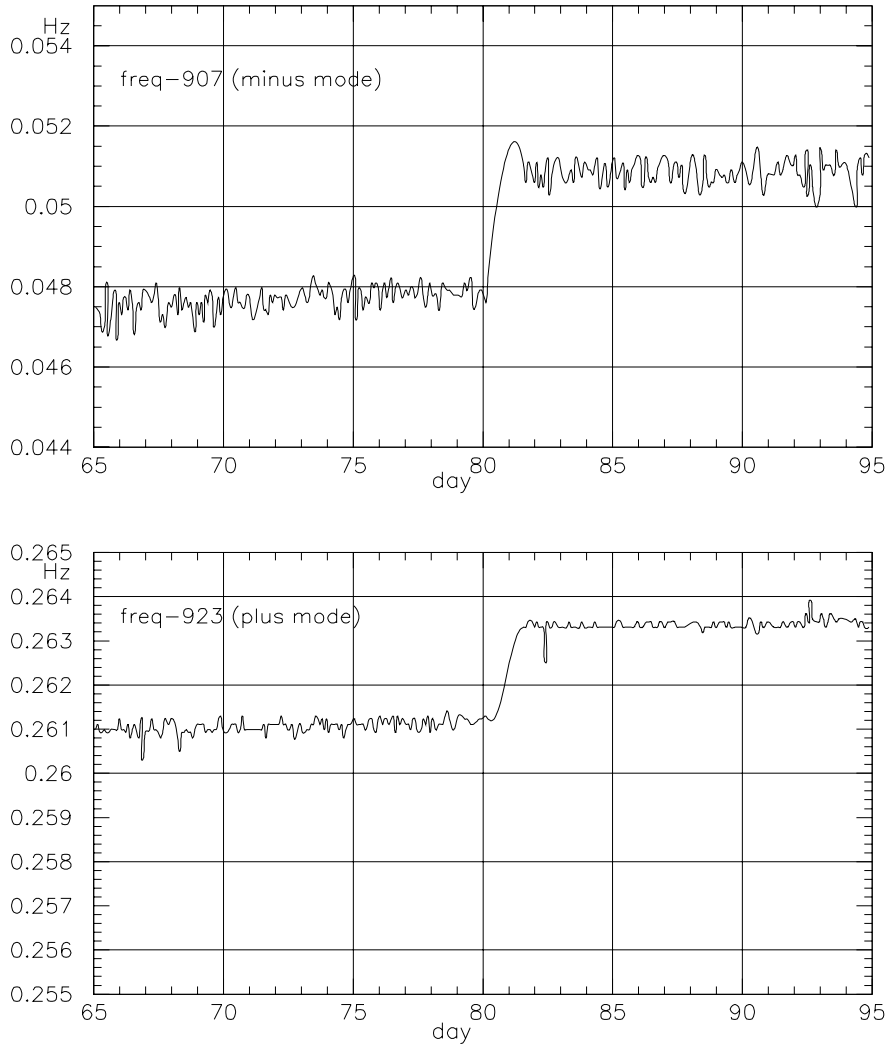

Fig. 29. – Resonance frequencies (Explorer 1994) of the two modes. It is possible to note a sharp variation occurring between the days 80 and 82.

described in paragraph **4**˙4.2 disappears and the effective temperature gets closer to its theoretical value.

APPENDIX A

The signal response after the matched filter.

We derive here the expressions for the quantities b' and d' considered in section **3**˙1. The solution of the quartic equation in (3.7) gives the following results for

the imaginary terms:

$$\text{(A.1)} \qquad \begin{cases} b = -\sqrt{|-e_0/\Delta_{12} - e_1 - \Delta_{12}/4|}\,, \\ d = -\sqrt{|+e_0/\Delta_{12} - e_1 - \Delta_{12}/4|}\,, \end{cases}$$

with e_0, e_1 functions of the coefficients M, N, O, L, P (see eq. (3.8))

$$\text{(A.2)} \qquad \begin{cases} e_0 = \dfrac{-MN/(2S_n m_y^2) + M^3/(8S_n^2 m_y^4) + O}{4S_n m_y^2}\,, \\ e_1 = \dfrac{8m_y^2 NS_n - 3M^2}{16S_n^2 m_y^4}\,. \end{cases}$$

It is useful to put the solutions in a polar form, that is

$$\text{(A.3)} \qquad \begin{cases} \omega_1^2 = \varrho(\cos\theta + j\sin\theta)\,, \qquad \omega_3^2 = \sigma(\cos\phi + j\sin\phi)\,, \\ \varrho = \sqrt{a^2 + b^2} \approx a\,, \qquad \sigma = \sqrt{c^2 + d^2} \approx c\,, \\ \theta = \operatorname{arctg}\dfrac{b}{a}\,, \qquad \phi = \operatorname{arctg}\dfrac{d}{c}\,. \end{cases}$$

Then

$$\omega_1 = \sqrt{\varrho}\left(\cos\frac{\theta}{2} + j\sin\frac{\theta}{2}\right) = a' + jb'\,,$$

$$\omega_3 = \sqrt{\sigma}\left(\cos\frac{\phi}{2} + j\sin\frac{\phi}{2}\right) = c' + jd'\,,$$

$$a' = \sqrt{\varrho}\cos\frac{\theta}{2}\,, \qquad b' = \sqrt{\varrho}\sin\frac{\theta}{2}\,,$$

$$c' = \sqrt{\sigma}\cos\frac{\phi}{2}\,, \qquad d' = \sqrt{\sigma}\sin\frac{\phi}{2}\,.$$

We have $b' \simeq \omega_+ \sin(\theta/2)$, with $\theta = \operatorname{arctg}(b/\omega_+^2)$ and $d' \simeq \omega_- \sin(\phi/2)$, with $\phi = \operatorname{arctg}(d/\omega_-^2)$.

For the two modes we obtain

$$\exp[-|b'||t|] \simeq \exp[-\omega_+ \sin(\theta/2)\,|t|]\,,$$

$$\exp[-|d'||t|] \simeq \exp[-\omega_- \sin(\phi/2)\,|t|]\,,$$

with $b' \simeq a\sin\theta/2$; $d' \simeq c\sin\phi/2$.

Let us now discuss the decay around one of the resonance frequencies, say ω_+. We have to study the function $\operatorname{arctg}(b/\omega_+^2)$. Our aim is to compare this decay with that obtained using the Wiener filter, applied after the lock-in amplifiers. We want to define a Γ equivalent parameter with a physical meaning similar to the spectral ratio Γ introduced in sect. **2**. We will call this dimensionless parameter Γ_3. In the tuned case we have $\beta_+ = \beta_-$ and $\beta_x = \beta_y$. By substituting eqs. (A.2) and (3.8) in eq. (A.1), we obtain

the following expression:

$$\text{(A.4)} \qquad b = -\left\{ \left| \frac{S_{fx}}{S_n} \frac{\mu^2 \alpha^2}{2 m_y^2} \left(\frac{2\beta^2}{\omega_0^2 \sqrt{\mu}} - \frac{1 + \sqrt{\mu} + \mu/4}{\sqrt{\mu}} \right) + \right. \right.$$

$$\left. \left. + \frac{S_{fy}}{S_n} \frac{\alpha^2}{2 m_y^2} \left(2 \frac{\beta^2 - \beta_x^2}{\omega_0^2 \sqrt{\mu}} - \frac{\sqrt{\mu} + \mu/4}{\sqrt{\mu}} \right) - 4 \frac{\beta^2 \omega_0^2}{\sqrt{\mu}} \left(\mu + \sqrt{\mu} \left(1 + \frac{\mu}{4} \right) \right) \right| \right\}^{1/2}$$

and, neglecting the β^2/ω_0^2 terms with respect to 1 and the last term of eq. (A.4) with respect to the first two terms

$$\text{(A.5)} \qquad b \simeq -\left\{ \left| -\frac{S_{fx}}{S_n} \frac{\mu^2 \alpha^2}{2 m_y^2} \left(\frac{1 + \sqrt{\mu} + \mu/4}{\sqrt{\mu}} \right) - \frac{S_{fy}}{S_n} \frac{\alpha^2}{2 m_y^2} \left(\frac{\sqrt{\mu} + \mu/4}{\sqrt{\mu}} \right) \right| \right\}^{1/2}.$$

Let us write b as

$$\text{(A.6)} \qquad |b| \simeq \beta_+^2 \left\{ \left| -\frac{S_{fx}}{S_n} \frac{\mu^2 \alpha^2}{2 m_y^2} \frac{1}{\beta_+^4} \frac{1 + \sqrt{\mu} + \mu/4}{\sqrt{\mu}} - \frac{S_{fy}}{S_n} \frac{\alpha^2}{2 m_y^2} \frac{1}{\beta_+^4} \frac{\sqrt{\mu} + \mu/4}{\sqrt{\mu}} \right| \right\}^{1/2}.$$

Recalling that $S_{fx} = 4kT\beta_x m_x$ and $S_{fy} = 4kT\beta_y m_y$, eq. (A.6) becomes

$$\text{(A.7)} \qquad |b| \simeq$$

$$\simeq \beta_+^2 \left\{ \frac{8kT_e \alpha^2 Q_+^2}{S_n \beta_+^2 m_x \Delta_{12}^2} \frac{\omega_x}{Q_x} \left(\frac{-(1 + \sqrt{\mu} + \mu/4)\, \omega_0^2 2\omega_0^2 \sqrt{\mu}}{\omega_+^2} + \frac{-(\sqrt{\mu} + \mu/4)\, \omega_0^2 2\omega_0^2 \sqrt{\mu}}{\mu \omega_+^2} \right) \right\} \simeq$$

$$\simeq \beta_+^2 \left\{ \frac{16kT_e \alpha^2 Q_+^2 \omega_+^2 \omega_x}{S_n m_x \Delta_{12}^2 Q_x \beta_+^2} \right\}.$$

So we may write

$$\text{(A.8)} \qquad b \simeq \beta_+^2 / \sqrt{\Gamma_{3+}},$$

where

$$\text{(A.9)} \qquad \Gamma_{3+} = \frac{S_n m_x \Delta_{12}^2 Q_x \beta_+^2}{16kT_e \alpha^2 Q_+^2 \omega_+^2 \omega_x}$$

is the requested dimensionless parameter.

Then the arctg argument is

$$b/\omega_+^2 = \beta_+^2 / (\omega_+^2 \sqrt{\Gamma_{3+}}).$$

We want to show now that, for $|b| \ll \omega_+^2$ (always true)

$$b' \simeq (1/2)\, b/\omega_+ \simeq \beta_+ / (\sqrt{\Gamma_+}).$$

The Γ_+ parameter is defined as the ratio of the wide-band noise S_n to the narrow-band noise spectrum S_{nb_+}. The latter may be obtained from the equation

$$S_{nb_+} = \alpha^2 S_{fx} |W_{ux}|^2 + \alpha^2 S_{fy} |W_{uy}|^2$$

evaluated at $\omega \simeq \omega_+$. Noticing that

$$|W_{ux}(\omega_+)|^2 \simeq (\omega_+^4 Q_+^2)/(m_x^2 \Delta_{12}^2 \omega_+^4)$$

and that

$$|W_{uy}(\omega_+)|^2 \simeq ((\omega_x^2 - \omega_+^2)^2 Q_+^2)/(m_y^2 \Delta_{12}^2 \omega_+^4)$$

we have, in the matched system,

$$S_{\mathrm{nb}_+} = \frac{\alpha^2 2kT_e Q_+^2}{m_x \Delta_{12}} \frac{\omega_x}{Q_x} \left(1 + \frac{\omega_0^4(\sqrt{\mu} + \mu/4)^2}{\mu \omega_+^4}\right) \simeq \frac{4\alpha^2 kT_e Q_+^2}{m_x \Delta_{12}^2} \frac{\omega_x}{Q_x} \tag{A.10}$$

(neglecting the terms μ and $\sqrt{\mu}$ with respect to the unit).

Then

$$\Gamma_+ \simeq \frac{S_n m_x \Delta_{12}^2 Q_x}{4\alpha^2 kT_e Q_+^2 \omega_x} \tag{A.11}$$

and, by comparing this equation with eq. (A.9),

$$\Gamma_{3+} \simeq \Gamma_+ \beta_+^2/(4\omega_+^2) = \Gamma_+/(16Q_+^2). \tag{A.12}$$

Finally

$$(1/2)\beta_+^2/(\omega_+ \sqrt{\Gamma_{3+}}) \simeq \beta_+/(\sqrt{\Gamma_+}).$$

For the decay around the other resonance frequency we obtain similar results:

$$d \simeq -\left\{\left| -\frac{S_{fx}}{S_n} \frac{\mu^2 \alpha^2}{2m_y^2} \left(\frac{-1 + \sqrt{\mu} - \mu/4}{\sqrt{\mu}}\right) - \frac{S_{fy}}{S_n} \frac{\alpha^2}{2m_y^2} \left(\frac{\sqrt{\mu} - \mu/4}{\sqrt{\mu}}\right)\right|\right\}^{1/2}, \tag{A.13}$$

$$d \simeq \beta_-^2/\sqrt{\Gamma_{3-}}, \tag{A.14}$$

with

$$\Gamma_{3-} = \frac{S_n m_x \Delta_{12}^2 Q_x \beta_-^2}{16kT_e \alpha^2 Q_-^2 \omega_-^2 \omega_x}, \tag{A.15}$$

$$d' \simeq (1/2)\, d/\omega_- \simeq \beta_-/(\sqrt{\Gamma_-}),$$

$$\Gamma_- \simeq \frac{S_n m_x \Delta_{12}^2 Q_x}{4\alpha^2 kT_e Q_-^2 \omega_x}. \tag{A.16}$$

REFERENCES

[1] ASTONE P., BASSAN M., BONIFAZI P., CARELLI P., CASTELLANO M. G., CAVALLARI G., COCCIA E., COSMELLI C., FAFONE V., FRASCA S., MAJORANA E., MODENA I., PALLOTTINO G. V., PIZZELLA G., RAPAGNANI P., RICCI F. and VISCO M., *Phys. Rev. D*, **47** (1993) 362.

[2] PALLOTTINO G. V., *Antenna gravitazionale con trasduttore risonante non accordato*, Internal report, IFSI-84-1 (1984).
[3] PALLOTTINO G. V. and PIZZELLA G., *Nuovo Cimento C*, **4** (1981) 237.
[4] PIZZELLA G., *Fisica Sperimentale del Campo Gravitazionale* (Nuova Italia Scientifica, Roma) 1993.
[5] PALLOTTINO G. V. and PIZZELLA G., *Data analysis and algorithms for gravitational wave antennas*, in *Data Analysis in Astronomy III*, edited by V. DI GESÙ (Plenum Press, New York) 1989, p. 361.
[6] ASTONE P., BONIFAZI P., PALLOTTINO G. V. and PIZZELLA G., *Nuovo Cimento C*, **17** (1994) 713.
[7] ASTONE P., BONIFAZI P., FRASCA S., PALLOTTINO G. V. and PIZZELLA G., *Nuovo Cimento C*, **15** (1992) 447.
[8] ASTONE P., FRASCA S., PALLOTTINO G. V. and PIZZELLA G., *A comparison between adaptive and non adaptive filters for gravitational wave antennas*, in *International Conference on Application of Time Series Analysis in Astronomy and Meteorology, Università di Padova* (*September 1993*).
[9] PAPOULIS A., *Probability, Random Variables, and Stochastic Processes* (McGraw-Hill, Singapore) 1984.
[10] FRASCA S., *The DAGA2 acquisition system for gravitational antennas*, in *International Conference on Application of Time Series Analysis in Astronomy and Meteorology, Università di Padova* (*September 1993*).
[11] TRETTER S. A., *Introduction to Discrete-Time Signal Processing* (John Wiley and Sons, New York) 1976.
[12] PAPOULIS A., *Signal Analysis* (McGraw-Hill, Singapore) 1977.
[13] ASTONE P., FRASCA S., PALLOTTINO G. V. and PIZZELLA G., *Comparison between different data analysis procedures for gravitational wave pulse detection*, in *Proceedings of the First Edoardo Amaldi Conference on Gravitational Wave Experiments, Rome, June 1994*, edited by E. COCCIA, G. PIZZELLA and F. RONGA (World Scientific) 1995.
[14] ASTONE P., BUTTIGLIONE C., FRASCA S., PALLOTTINO G. V. and PIZZELLA G., *Algorithms for gravitational wave data analysis*, in *Proceedings of XI Italian Relativity Meeting, Trieste, September 1994*, edited by M. CARFORA *et al.* (World Scientific) 1996.